environmental microbiology

Environmental Microbiology (2017) **00**(00), 00–00 doi:10.1111/1462-2920.13996

Interrogating marine virus-host interactions and elemental transfer with BONCAT and nanoSIMS-based methods

Alexis L. Pasulka,[1†] Kimberlee Thamatrakoln,[2] Sebastian H. Kopf,[3] Yunbin Guan,[1] Bonnie Poulos,[4] Annie Moradian,[5] Michael J. Sweredoski,[5] Sonja Hess,[5‡] Mathew B. Sullivan,[6] Kay D. Bidle[2] and Victoria J. Orphan[1]

[1]*Division of Geological and Planetary Sciences, California Institute of Technology, CA, USA.*

[2]*Department of Marine and Coastal Studies, Rutgers University, NJ, USA.*

[3]*Department of Geological Sciences, University of Colorado Boulder, CO, USA.*

[4]*Department of Ecology and Evolutionary Biology, University of Arizona, AZ, USA.*

[5]*Proteome Exploration Laboratory, California Institute of Technology, CA, USA.*

[6]*Department of Microbiology, Ohio State University, OH, USA.*

Summary

While the collective impact of marine viruses has become more apparent over the last decade, a deeper understanding of virus-host dynamics and the role of viruses in nutrient cycling would benefit from direct observations at the single-virus level. We describe two new complementary approaches – stable isotope probing coupled with nanoscale secondary ion mass spectrometry (nanoSIMS) and fluorescence-based biorthogonal non-canonical amino acid tagging (BONCAT) – for studying the activity and biogeochemical influence of marine viruses. These tools were developed and tested using several ecologically relevant model systems (*Emiliania huxleyi*/EhV207, *Synechococcus sp.* WH8101/Syn1 and *Escherichia coli*/T7). By resolving carbon and nitrogen enrichment in viral particles, we demonstrate the power of nanoSIMS tracer experiments in obtaining quantitative estimates for the total number of viruses produced directly from a particular production pathway (by isotopically labelling host substrates). Additionally, we show through laboratory experiments and a pilot field study that BONCAT can be used to directly quantify viral production (via epifluorescence microscopy) with minor sample manipulation and no dependency on conversion factors. This technique can also be used to detect newly synthesized viral proteins. Together these tools will help fill critical gaps in our understanding of the biogeochemical impact of viruses in the ocean.

Received 8 August, 2017; revised 10 November, 2017; accepted 12 November, 2017. Present addresses: [†]Biological Sciences Department, California Polytechnic State University, San Luis Obispo, CA, USA; [‡]Antibody Discovery and Protein Engineering, Medimmune, Gaithersburg, MD, USA

Introduction

Marine viruses impact food webs by shaping microbial community structure, serving as agents of gene transfer and altering the direction and magnitude of carbon and nutrient flow (Fuhrman, 1999; Wommack and Colwell, 2000; Suttle, 2007; Weitz and Wilhelm, 2012). These microscopic predators infect the oceanic primary producers (e.g., *Prochlorococcus*, *Synechococcus*, Sullivan *et al.*, 2003 and eukaryotic phytoplankton, Brussaard, 2004a) and nitrogen fixers (e.g., *Trichodesmium*, Hewson *et al.*, 2004), as well as globally dominant pelagic (SAR11, Zhao *et al.*, 2013 and SAR116, Kang *et al.*, 2013) and particle-associated heterotrophic bacteria (Bacteriodetes, Holmfeldt *et al.*, 2013) and grazers (Massana *et al.*, 2007).

Recent technological advances have changed our ability to study and understand the ecology of marine viruses (Brum and Sullivan, 2015). Metagenomics has enabled scientists to have a better understanding of viral diversity and biogeography (Angly *et al.*, 2006; Brum *et al.*, 2015) as well as the predictive power to connect viruses with their hosts at larger community scales (Edwards *et al.*, 2015; Roux *et al.*, 2016a,b). However, quantitative estimates of viral-induced mortality and the degree to which carbon and nutrients are cycled through virioplankton remain poorly constrained. Our current estimates of viral mortality are based primarily on indirect inferences and modelling (reviewed in Fuhrman, 1999; Wommack and Colwell, 2000; Suttle, 2005; Breitbart *et al.*, 2008) and are

insufficient to capture the spatial and temporal variability needed to properly incorporate viruses into global ocean models (Weitz *et al.*, 2014). Furthermore, the viral shunt paradigm – the idea that viral lysis will 'keep carbon small' by reducing the flow of carbon moving upwards in the food web (Wilhelm and Suttle, 1999; Suttle, 2007; Weitz and Wilhelm, 2012) – remains virtually unquantified due to technical challenges of making such measurements in natural populations. Recent measurements hint that virus-infected cells may be preferentially grazed (Evans and Wilson, 2008; Frada *et al.*, 2014) and that viruses, better than prokaryotes and eukaryotes, predict 89% of variability in global ocean carbon flux from the surface waters to the deep sea – with cyanophages the best predictor among them (Guidi *et al.*, 2016). As the decades-old viral shunt paradigm is being reevaluated with conceptual models (Weinbauer, 2004), and with new data suggesting that viruses can increase, rather than decrease carbon export in the oceans (Vardi *et al.*, 2012; Guidi *et al.*, 2016), independent quantitative methods to assess viral activity and their biogeochemical influence is critical.

The development and application of single-cell resolved isotopic (nano-scale secondary ion mass spectrometry or nanoSIMS) and fluorescence-based activity (biorthogonal non-canonical amino acid tagging or BONCAT) approaches in microbial ecology have enabled scientists to directly track cell-specific microbial activity and associated influence on biogeochemical cycling in an environmental context (e.g., Musat *et al.*, 2008; Dattagupta *et al.*, 2009; Sheik *et al.*, 2013; 2014; Kopf *et al.*, 2015; Terrado *et al.*, 2017). While the 50 nm spatial resolution of the nanoSIMS is technically sufficient for resolving individual viruses, the combination of stable isotope probing and nanoSIMS has not yet been tested for the study of carbon and nitrogen transfer between environmental viruses and their host microorganisms. More recently, the BONCAT method (Dieterich *et al.*, 2006) coupled with fluorophore addition via copper catalysed 'click chemistry' has been used to visualize translationally active microorganisms in diverse environments (Hatzenpichler *et al.*, 2014; 2016; Samo *et al.*, 2014); however, the adaptation of BONCAT for fluorescently tracking virus-host interactions and rates of viral production has not been explored.

In this study, we tested the feasibility and constraints of using BONCAT and nanoSIMS to directly quantify new viral production and the transfer of carbon and nitrogen from host to virus during cell lysis. These methods were validated using 3 virus-host model systems including: *Emiliania huxleyi* strain CCMP374 and its ~ 200nm coccolithovirus EhV207, *Synechococcus sp.* strain WH8101 and its ~ 80nm virus Syn1 and *Escherichia coli* and its ~ 50 nm phage T7 with an eye towards laying a foundation for interrogating virus-host interactions within complex microbial communities. These specific model systems were selected because their infection dynamics are well characterized and, in the case of EhV207 and Syn1, they represent ecologically relevant marine virus-host pairs. The use of stable isotope probing coupled to nanoSIMS analysis extends the ability to study the flow and fate of carbon and nitrogen through the smallest active members of marine food webs. Viral BONCAT shows promise as a fluorescence-based microscopy method for directly quantifying the proportion of newly synthesized lytic viruses (i.e., viral production), extending the utility of relatively rapid, viral-targeted DNA stains and epifluorescence microscopy assays (Hara *et al.*, 1991; Noble and Fuhrman, 1998). Taken together, these new single viral particle resolved isotopic and fluorescence-based assays will help fill critical gaps in our understanding of the activity and biogeochemical impact of viruses in ocean ecosystems.

Results

Quantification of stable isotopes in viral particles using stable isotope probing and nanoSIMS

In both the cyanobacterial and eukaryotic algal-virus model systems, we were able to visualize enrichment in carbon-13 and nitrogen-15 in individual viral particles on the nanoSIMS and trace the transfer of ^{13}C (bicarbonate) and ^{15}N (nitrate or ammonium) incorporated by the photosynthetic hosts to their viruses after host lysis (Fig. 1). Both sets of virus-host pairs showed enrichment in stable isotope amended treatments relative to unlabelled controls (Figs. 2–4). As a result of slight differences in the length of time grown in the presence of the isotopically labelled substrate (see *Methods* for details), *Synechococcus sp.* and *E. huxleyi* C and N enrichment varied across different experiments. However, independent of the absolute level of enrichment detected, the transfer of ^{13}C and ^{15}N-labelled biomolecules from host to newly synthesized viral particles was reproducible (Figs. 2–4) in both single and dual isotope (^{13}C and ^{15}N) labelling experiments.

For both model systems the isotopic enrichment in the viral particles was similar to that of the host whenever the host culture was fully acclimated to isotopically labelled nutrients (Figs. 2 and 4). *Synechococcus sp.* cells and Syn1 particles (~80 nm capsid) recovered from stable isotope probing experiments with ^{13}C-bicarbonate, had an average fractional abundance ($^{13}C/^{13}C+^{12}C$) of 21 ± 1.0 at % (atom percent) and 15 ± 4.7 at% ^{13}C respectively, approximately 15 times greater than natural abundance (~1.1 at% ^{13}C; Fig. 2, Exp.1). After amendment with ammonium (^{15}N-labelled), measured populations of *Synechococcus sp.* and Syn1 had an average fractional abundance of 63 ± 1.7 at% and 75 ± 7.1 at% ^{15}N (Exp. 2) and 82 ± 2.0 at% and 69 ± 8.5 at% ^{15}N (Exp. 3) respectively, approximately 200 times over the natural abundance value of ~0.36 at% ^{15}N (Fig. 2). NanoSIMS analysis of

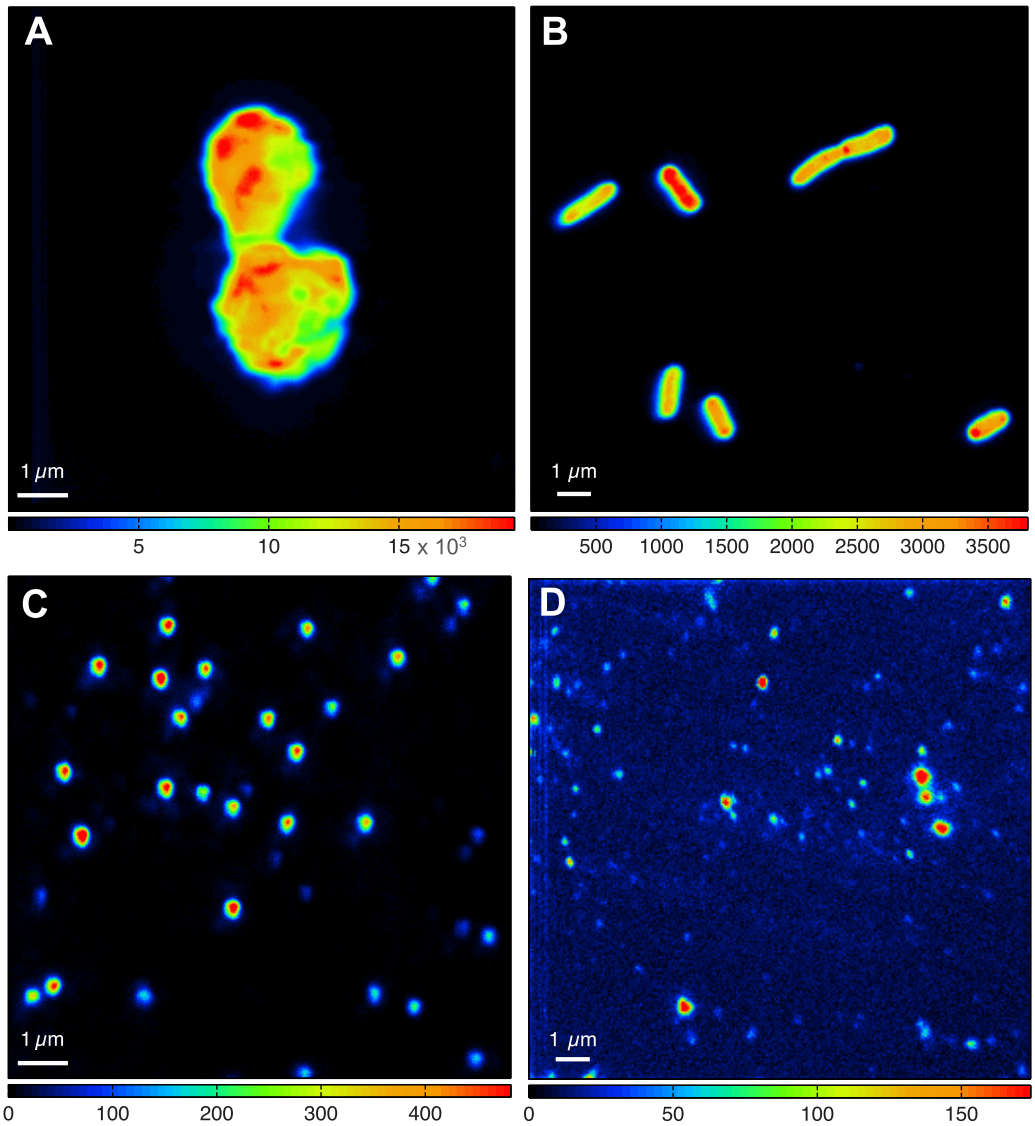

Fig. 1. NanoSIMS ion images of cultured hosts and viruses. Example ion images ($^{14}N^{12}C$-) of *Emiliania huxleyi* 374 (A), *Synechococcus* WH8101 (B), EhV 207 (C) and Syn1 (D). Colour scale represents total ion counts. Large particles in D are gold beads.

Synechococcus sp. and Syn1 from unlabelled control experiments demonstrated these particles had fractional abundances close to natural abundance (*Synechococcus sp.* was 1.11 ± 0.03 at% ^{13}C and 0.365 ± 0.02 at% ^{15}N; Syn1 was 1.19 ± 0.07 at% ^{13}C and 0.37 ± 0.19 at% ^{15}N for ^{13}C and ^{15}N respectively).

After incubation with ^{13}C-bicarbonate, *E. huxleyi* and its virus EhV207 (~200 nm capsid) had an average fractional abundance of 30 ± 1.3 at% and 30 ± 4.1 at% ^{13}C respectively, approximately 30 times over natural abundance (Fig. 3, Exp.1) and after incubation with ^{15}N-nitrate, the eukaryotic host and recovered EhV207 virus had an average fractional abundance of 81 ± 2.0 at% and 72 ± 2.7 at% ^{15}N respectively, approximately 200 times over natural abundance (Fig. 3, Exp. 2). After incubation with both ^{13}C-bicarbonate and ^{15}N-nitrate, *E. huxleyi* and EhV207 had an average ^{13}C fractional abundance of 15 ± 1.0 at% and 15 ± 2.9 at% ^{13}C respectively, and an average ^{15}N fractional abundance of 95 ± 1.2 at% and 85 ± 2.5 at% ^{15}N respectively (Fig. 3, Exp. 3). *E. huxleyi* and EhV in unlabelled controls remained at natural abundance (*E. huxleyi* fractional abundances were 1.1 ± 0.07 at% ^{13}C and 0.37 ± 0.007 at% ^{15}N; EhV207 fractional abundances were 1.0 ± 0.27 at% ^{13}C and 0.37 ± 0.07 at% ^{15}N).

Short-term (24-h) stable isotope probing experiments conducted with *Synechococcus sp.* and its virus Syn1 (Fig. 4) are more analogous to the type of experiment possible in the field. Even with this relatively short-term incubation, detection of the transfer of ^{13}C and ^{15}N-labelled macromolecules between host and virus was possible by nanoSIMS.

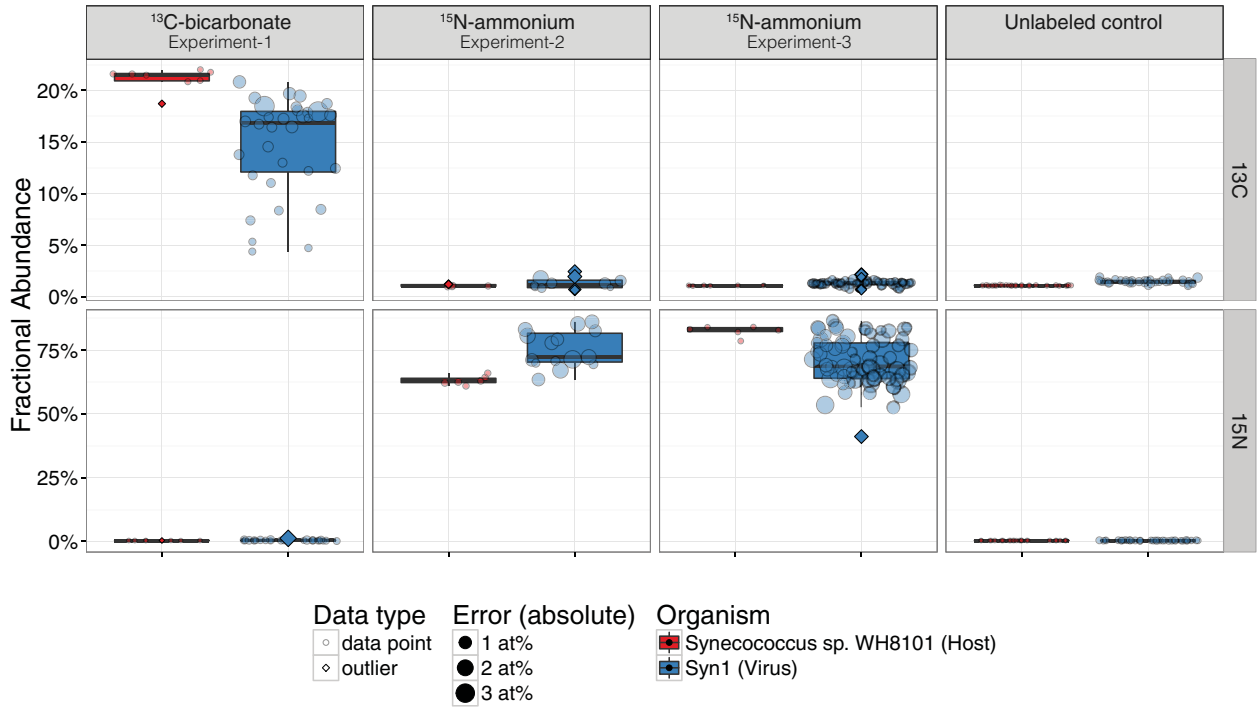

Fig. 2. Compiled nanoSIMS data from single-label experiments with cyanobacterial-virus model system. Whisker plots showing fractional abundance of *Synechococcus sp.* WH8101 and virus Syn1 after incubation with ^{13}C-bicarbonate (Exp. 1), ^{15}N-ammonia (Exps. 2, 3) and control incubations (right panel). Fractional abundance (*y*-axis) reveals enrichment above background for carbon (top row, natural = 1.09 at %) and nitrogen (bottom row, natural = 0.36 at %).

Notably, there was an offset in ^{15}N-enrichment between paired host and virus (with greater enrichment in the virus), with *Synechococcus sp.* and Syn1 containing an average fractional abundance of 19 ± 2.8 at% and 64 ± 4.9 at% ^{15}N respectively. This offset was not observed in the acclimated Synechococcus cultures grown for multiple generations in the presence of the isotope label (Fig. 2).

The potential for abiotic adsorption of the ^{15}N-labelled nitrate and ammonium to the cell surface was experimentally tested in formaldehyde killed controls and determined to be minimal, with no significant contribution to the experimental enrichment signal (Supporting Information Fig. S2). These findings are consistent with the results from SIMS $^{15}NH_4$ adsorption control experiments reported in Orphan and colleagues (2009) and Dekas and colleagues (2009).

Viral particles had significantly lower ion counts (within an analytical frame as well as across analytical frames) relative to the host cells (Fig. 1, Supporting Information Fig. S3). The larger eukaryotic viral particles (~200 nm, EhV207) generated an average of 582 and 583 ^{12}C− and ^{14}N^{12}C− counts per particle per frame while the smaller viral particles (~70 nm, Syn1) yielded an average of 438 and 209 ^{12}C− and ^{14}N^{12}C− counts per particle per frame. Host cyanobacteria and algal cells had much higher average C and N counts per cell per frame (*E. huxleyi* = 8.7 × 10^5 ^{12}C−, 13.5 × 10^5 ^{14}N^{12}C−; *Synechococcus sp.* = 8.8 × 10^4 ^{12}C−, 2.3 × 10^5 ^{14}N^{12}C−), consistent with increased biovolume. As a result of the low ion yield for the submicron viral particles, the statistical error for our virus stable isotope ratios was much larger than for host cells (See Supporting Information Appendix S1 for details on error propagation). Merging data across multiple analytical frames increased the total counts to 10^4 and 10^3 for EhV207 and Syn1 respectively, reducing the error around each estimate (Supporting Information Fig. S3 and Appendix S1). Overall, our data indicate that the propagated relative error (1σ) from counting statistics on the ^{13}C and ^{15}N fractional abundance estimate of an individual viral particle ranges between 1 and 3 atom % (Figs. 2–4). The total diversity (population standard deviation) in the fractional abundance isotopic composition of the viral particles in each tracer acclimated culture system ranged from 2.5%–3.7% for EhV207 (n = 214 particles measured) and 4.9%–9.7% for Syn1 (n = 260 particles measured). See Supporting Information Appendix S4 for additional details on methodological considerations for viral isotope measurements.

Viral-BONCAT: detection of HPG incorporation in cultured virus-host models using epifluorescence microscopy

BONCAT coupled with fluorophore addition via copper (I)-catalysed azide-alkyne cycloaddition (i.e., click chemistry)

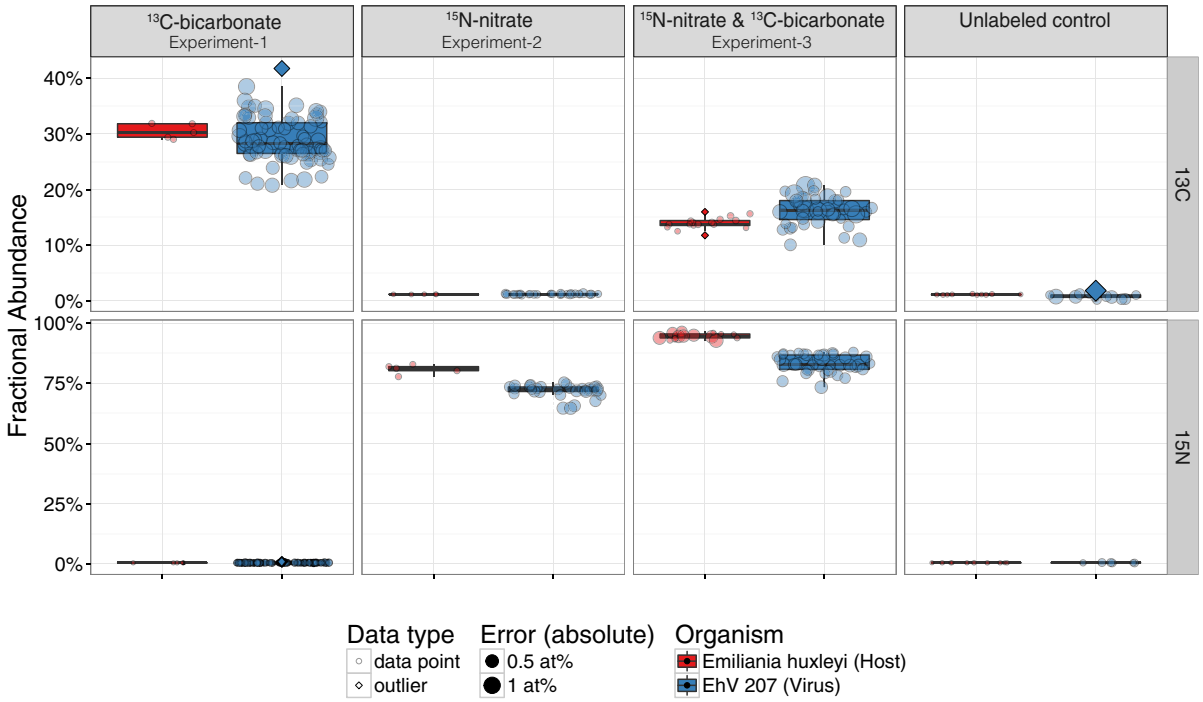

Fig. 3. Compiled nanoSIMS data from single and dual label experiments with eukaryotic algae-virus model system. Whisker plots showing fractional abundance data from single-label (Exp. 1,2) and dual-label (Exp. 3) incubations with coccolithophore *E. huxleyi* and its virus EhV 207 after incubation with ^{15}N-nitrate and/or 13C-bicarbonate as well as control incubations (right panel). Fractional abundance (*y*-axis) reveals enrichment above background for carbon (top row, natural = 1.09 at %) and nitrogen (bottom row, natural = 0.36 at %).

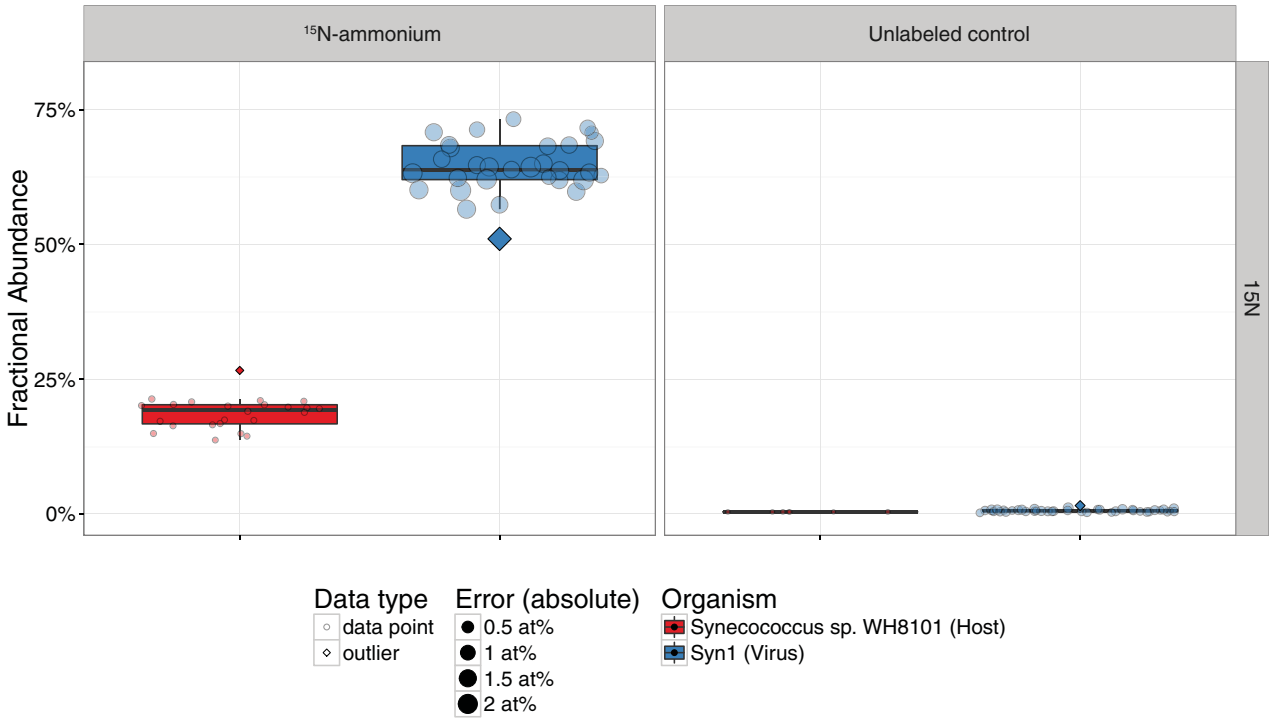

Fig. 4. Compiled nanoSIMS data from short-term experiments with cyanobacterial-virus model system. Whisker plots showing fractional abundance of *Synechococcus sp.* WH8101 and virus Syn1 after incubation with ^{15}N-ammonia (left panel) for 24 h. An unlabelled control incubation (right panel) was run in parallel. Fractional abundance (*y*-axis) reveals enrichment above background for nitrogen (natural = 0.36 at %).

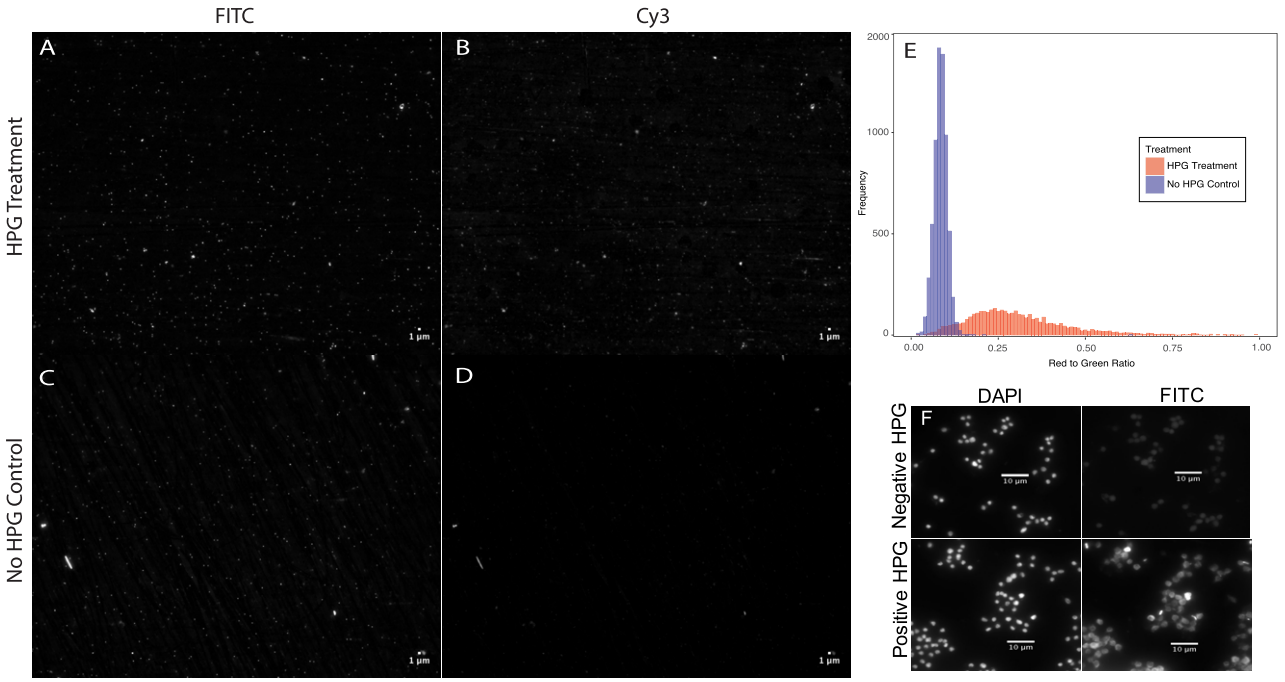

Fig. 5. Visualization of BONCAT labelled *E. huxleyi* virus (EhV 207) and fluorescence analysis. Examples of images of EhV particles from experiments of *E. huxleyi* grown with (A, B) and without (C, D) HPG. The click reaction was performed with a TAMRA-Azide dye (detected with a Cy3 filter cube) and particles were counter stained with SYBR gold (detected with a FITC filter cube). Histogram (E) the red to green fluorescence ratio (*R:G*) of viral particles from all particles analysed across 16 images (viral particles $n_{HPG} = 3713$, $n_{CONTROL} = 6522$). Red bars are from particles in the HPG labelled treatment, and blue bars are from viral particles in the no HPG control. (F) Visualization of BONCAT labelled *E. huxleyi* compared to no HPG control. The click reaction was performed with CR-110-Azide dye (detected with FITC filter cube) and cells were counter stained with DAPI (detected with a DAPI filter cube). Note. Images in figure have been background corrected.

was used successfully to demonstrate the transfer of HPG, a methionine analogue, from newly synthesized proteins in cultured host cells to their viruses during lytic infection. Initial BONCAT experiments were conducted with co-cultures of *E. huxleyi* and its virus EhV207 as well as with *E. coli* and an infecting T7 phage. Incorporation of HPG by host cells (*E. huxleyi* and *E. coli*) was confirmed by epifluorescence microscopy using standard BONCAT protocols (Hatzenpichler *et al.*, 2014; Figs. 5F and 6F). Consistent with previous reports, HPG addition (100 μM final concentration) did not significantly alter host growth relative to incubations without HPG (Supporting Information Fig. S4; Dieterich *et al.*, 2006; Bagert *et al.*, 2014; Hatzenpichler *et al.*, 2014; 2016). After lysis of HPG-labelled host lysis, individual viral particles were analysed for incorporation of HPG using our modified BONCAT protocol and visualized by epifluorescence microscopy. The fluorescence intensity and number of viral particles were quantified from digital images by measuring the fluorescence signal of the azide-containing TAMRA fluorophore (R = click signal in Cy3) relative to the fluorescence signal from the SYBR Gold (G = DNA signal in FITC) within individual viral particles. Fluorescence image analysis of T7 (50 nm), Syn1 (80 nm) and EhV (200 nm) confirmed that individual viral particles across a range of sizes could be identified in digital images based on their FITC signal from SYBR Gold stain (Supporting Information Fig. S5). These cultured viruses were also used to determine an appropriate size cutoff that could be applied during digital image analysis. The minimum size for all viruses considered was constrained to 1 pixel (0.1159 μm) determined by CCD camera resolution (QIClick 12bit) and we conservatively chose an upper size limit of 0.45-μm (approximately 4 pixels; Supporting Information Fig. S5) to capture viral particles that were < 200 nm. While these sizes are not reflective of actual capsid size, our analyses show that the application of these cutoffs effectively captured the particle size range of interest (Supporting Information Fig. S5).

The red-to-green (BONCAT-cy3/DNA-Sybr Gold) fluorescence ratios (*R:G*) of all viral particles were pooled within treatments to compare the distribution of *R:G* ratios across treatments (Figs. 5 and 6). For both the EhV and T7 populations, a higher *R:G* ratio was observed in viral particles produced from host cultures incubated with HPG relative to the negative controls (host incubation without HPG) (mean (μ); $\mu_{HPG} = 0.31$, $\mu_{NEG} = 0.08$ and $\mu_{HPG} = 0.68$, $\mu_{NEG} = 0.09$ for EhV and T7 respectively). Wilcoxon Rank-Sum test was used to confirm the negative control and positive treatment distributions were significantly different from one another (p values < 0.05). Using probability statistics

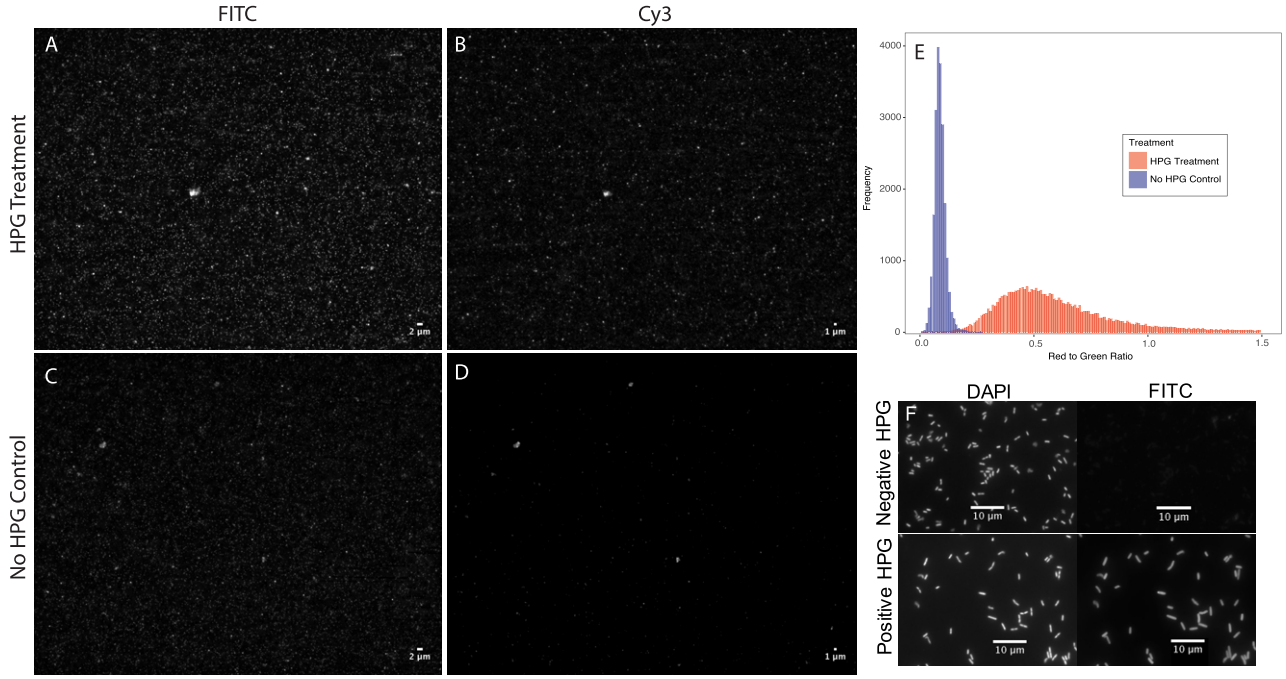

Fig. 6. Visualization of BONCAT labelled *E. coli* virus (T7) and fluorescence analysis. Examples of images of T7 particles from experiments of *E. coli* grown with (A, B) and without (C, D) HPG. Click reaction was performed with a TAMRA-Azide dye (detected with a Cy3 filter cube) and particles were counter stained with SYBR gold (detected with a FITC filter cube). Histogram (E) of the red to green fluorescence ratio (*R:G*) of viral particles from all particles analysed across 10 images (viral particles $n_{HPG} = 31\,512$, $n_{CONTROL} = 20\,858$). Red bars are from particles in the HPG labelled treatment, and blue bars are from viral particles in the no HPG control. (F) Visualization of BONCAT labelled *E. coli* compared to no hPG control. The click reaction was performed with CR-110-Azide dye (detected with FITC filter cube) and cells were counter stained with DAPI (detected with a DAPI filter cube). Note. Images in figure have been background corrected.

coupled to bootstrapping, we estimated the percentage of newly synthesized particles. For T7, 99.2% of viral particles were designated as HPG-labelled (e.g., newly synthesized) with a lower and upper 95% confidence interval of 98.9% and 99.4% respectively. For the eukaryotic virus EhV, 94.5% of viral particles were designated as HPG-labelled (e.g., newly synthesized) with a lower and upper estimate of 91.2% and 97.2% respectively.

Detection of HPG incorporation into newly synthesized viral proteins via proteomics

To independently confirm the successful transfer of host-associated HPG-labelled proteins or peptides into infecting viral particles, we conducted proteomic experiments on BONCAT-labelled *E. coli* T7 and *E. huxleyi* EhV207 and ran a targeted screen for HPG-labelled viral proteins. Proteomic analysis of the concentrated viral lysates confirmed the incorporation of HPG into select viral proteins. Here positive identification of peptide-spectrum matches was determined where the methionine (Met) in the peptide was replaced with an HPG, which results in a −21.9877 Da mass shift.

In the *E. coli* and T7 BONCAT experiment, 8 different T7 proteins associated with viral particle structure (e.g., procapsid and capsid formation as well as packaging the DNA into the capsid) were found to contain 12 HPG substitutions (Table 2). For the *E. huxleyi* and EhV 207 BONCAT experiment, 5 different EhV 207 proteins, including the major capsid protein and several putative uncharacterized proteins, were observed to contain 6 HPG substitutions. The annotated spectra for the HPG-labelled proteins are available in Supporting Information Appendix S3. The mass spectrometry proteomics data have been deposited to the ProteomeXchange Consortium via the PRIDE (Vizcaíno *et al.*, 2016) partner repository with the data set identifier PXD006580.

Table 1. Comparison of BONCAT and nanoSIMS approaches for studying viral interactions.

	BONCAT	nanoSIMS
Benefit	Assessment of production	Assessment of C and N transfer from host to virus
Quantitative	Semiquantitative	Quantitative
Throughput	High	Low
Cost	Inexpensive	Expensive
Limitations	Requires host to assimilate HPG	Lower size limit (20–50 nm)

Table 2. Proteomics identification of HPG-labelled T7 and EhV proteins from Viral BONCAT experiments.

Virus	Protein name	Protein	HPG-substitution positions
T7[a]	Major capsid protein 10A;Minor capsid protein 10B	P19726;P19727	1;4;10;293
T7	DNA ligase	P00969	288
T7	Capsid assembly scaffolding protein (Gp9)	P03716	279
T7	Terminase, small subunit gp18	P03693	22
T7	Single-stranded DNA-binding protein gp2.5	P03696	137
T7	Peptidoglycan hydrolase gp16	P03726	150
T7	Portal protein	P03728	118;179
T7	Protein 6.5	P03800	1
EhV[b]	Major capsid protein	G4YBV8	23
EhV	Putative uncharacterized protein	G4YBJ4	97;105
EhV	Putative uncharacterized protein	G4YBX3	97
EhV	Putative uncharacterized protein	G4YCD5	91
EhV	Putative uncharacterized protein	G4YCE6	39

a. Source for T7 proteins: http://www.uniprot.org/uniprot/?query=organism:10760+keyword:1185
b. Source for EhV 207 proteins: https://www.ncbi.nlm.nih.gov/nuccore/JF974317.1.

Sensitivity of fluorescence detection for Viral BONCAT

In BONCAT, the fluorescence intensity should be proportional to the total number of HPG substitutions for methionine within the viral proteome after the incubation. To assess the sensitivity of the BONCAT fluorescence assay to resolve newly synthesized viral particles, we ran an *in silico* analysis examining the influence of the number of Met substitutions and the *R:G* ratio shift per substitution on the resultant *R:G* distributions (Supporting Information Figs. S6 and S7). By combining the T7 proteomics data with the *R:G* ratio distributions from the ~50 nm T7 particles after BONCAT labelling, we derived estimates for the number of detected substitutions (n_{subs}) and the impact of an HPG substitution on the *R:G* ratio (*d*RG). 12 HPG substitutions were detected in the T7 proteome with a corresponding estimated mean shift in *R:G* ratio of $dRG = 0.049$ per substitution (based on the mean difference in *R:G* between HPG labelled sample and negative control). Assuming substitutions are binomially distributed, the number of average substitutions affected the shape of the expected *R:G* histogram, with an increasing number of substitutions leading to a wider *R:G* spread (Supporting Information Fig. S6). We also observed a shift in the HPG-positive distribution by accounting for different levels of variability around the *d*RG (Supporting Information Fig. S7). A higher level of variation (i.e., 60%) resulted in a distribution with a more skewed tail.

To test our ability to accurately measure viral production, we modelled our T7 BONCAT data assuming a specific level of activity (e.g., the percent of the viral population actively turning over) across a wide range of the aforementioned parameters, and then determined if it was possible to back calculate the starting activity levels using the rank-sum based activity statistic (see Supporting Information Appendix S2 for more details) without prior knowledge of the input parameters (Fig. 7). This exercise revealed that it is possible to accurately estimate the number of newly synthesized viral particles using Viral-BONCAT in situations where >25% of the viral population is actively turning over and there is >1 methionine substitution per viral particle with a resulting shift in *R:G* per substitution (*d*RG) of > 0.03 (Fig. 7, Supporting Information Figs. S6 and S7). Below this level of substitution and population turnover, we were unable to accurately calculate viral activity, as the small shift in the *R:G* per substitution resulted in greater error around the production measurement (Fig. 7). Accurate estimates of production can be derived with a *d*RG of 0.01, as long as there are a greater number of substitutions per viral particle (i.e., $n_{subs} \geq 5$), or the fraction of the population turning over is higher (i.e., % active ≥ 25%). This distinction between 'background noise' (e.g., BONCAT negative distributions) and the distribution associated with BONCAT positive particles becomes even more pronounced with higher *d*RGs (on the order of the 0.049 observed for T7; Supporting Information Figs. S6 and S7). Based on our observations from treatment replicates, we also determined how systematic error in the observed *R:G* ratios due to systemic shift in signal intensity of the measured green fluorescence in either the samples themselves, or in the positive control, could limit the ability to measure viral production using BONCAT (Supporting Information Fig. S8). While the limitations of a low number of substitutions and/or low *R:G* shifts per substitution remain the same, taking this systematic error into consideration increases the confidence intervals for the activity estimates.

Estimating viral production from BONCAT

Incubations using coastal seawater amended with HPG (100 μM) were conducted to assess the utility of Viral-BONCAT for estimating viral production in the field. In

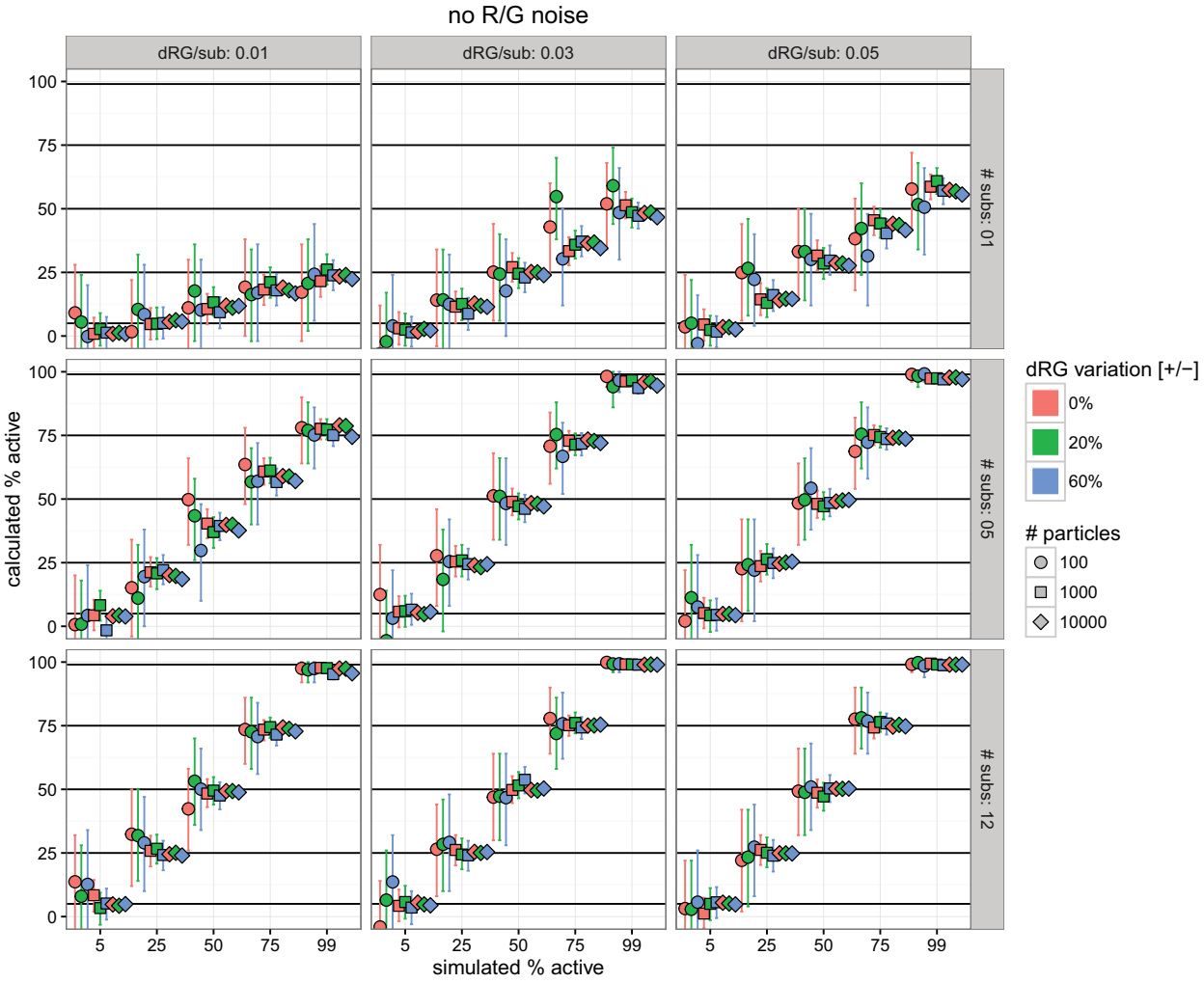

Fig. 7. Accuracy and precision of viral production estimates using Viral BONCAT. Results from modelling T7 data with a specific level of activity (e.g., the percent of the population actively turning over) and varying n_{sub}, *d*RG and different levels of variability around the *d*RG to determine the ability to back calculate the original activity using the rank-sum bootstrap approach.

these experiments, the starting virus concentration was $2.63 \times 10^7 \pm 2.21 \times 10^6$ particles ml^{-1}. After 48 hours and 72 hours, virus concentrations were $2.72 \times 10^7 \pm 5.55 \times 10^6$ and $2.30 \times 10^7 \pm 5.08 \times 10^6$ particles ml^{-1} (averages of replicates) respectively. Histograms of *R:G* ratios revealed that the population of viruses produced in the HPG treatments had a higher mean *R:G* ratio relative to the negative controls after 48 and 72 hours ($\mu_{HPG} = 0.2$, $\mu_{NEG} = 0.1$; Fig. 8, Table 3). A Wilcoxon rank-sum test was used to confirm the negative control and positive HPG treatment distributions were significantly different from one another (*p* values < 0.05). We observed greater overlap in the *R:G* ratios between the negative controls and the HPG treatments from the field experiments compared to the Viral-BONCAT with our cultured model organisms. There was also a significant difference in *R:G* ratio distributions in HPG treatments between 48 hours and 72 hours (*p* value < 0.05). Using probability statistics coupled to bootstrapping, we estimated the number of newly synthesized particles at each time point (combining both replicates). After 48 hours, 85.8% of viral particles were designated as HPG-labelled (e.g., newly synthesized) with a lower and upper 95% confidence interval of 78.7% and 91.1% respectively. After 72 hours, 78.5% of viral particles were designated as HPG-labelled (e.g., newly synthesized) with a lower and upper 95% confidence interval of 68.2% and 86.7% respectively. Virus production rates (calculated from the 48-h data only) were estimated be 16.4×10^6 particles ml^{-1} day^{-1} translating to a viral turnover of 1.5 days (Table 4).

Discussion

Viruses are integral to microbial food webs and play an important role in the fate and cycling of carbon and

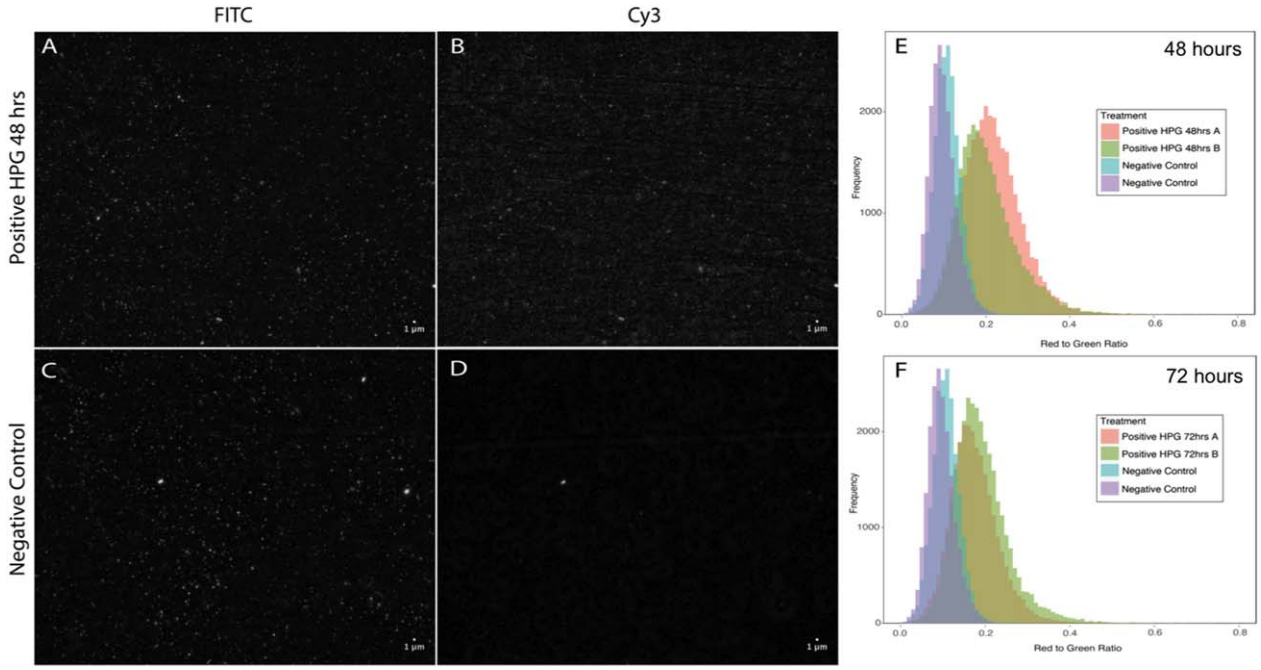

Fig. 8. Visualization of BONCAT labelled viruses and fluorescence analysis from field tests. Fluorescence images of viral particles from field experiment in which seawater was amended with HPG for 48 h (example images shown in A, B) and 72 h (images not shown) relative to the negative control (example images shown C, D). Click reaction was performed with a TAMRA-Azide dye (detected with a Cy3 filter cube) and particles were counter stained with SYBR gold (detected with a FITC filter cube). Histograms of red to green fluorescence ratio of viral particles incubated with HPG after 48 h (E) and 72 h (F). The colour of the bar indicates treatment. See Table 2 for details on percentage of viral particles labelled and number of particles analysed. Note. Images in figure have been background corrected.

nutrients in the ocean. While our understanding of the impact of viruses in ocean ecosystems has increased through the use of metagenomics, model systems and microscopy, we currently lack methods to directly assess the rates of new virus production and the transfer of carbon and nitrogen derived from active microbial host cells. This study introduces two complementary microanalytical imaging methods using nanoSIMS and BONCAT that address this knowledge gap, enabling the direct quantification of newly synthesized viral particles and information about host-derived carbon and nitrogen sources within environmental samples. The ability to fluorescently tag newly synthesized host and viral proteins by BONCAT directly in environmental samples represents an easy to implement and versatile method for quantifying new viral production by epifluorescence microscopy. Likewise, the analyses of Carbon-13 and/or Nitrogen-15 enrichment in viral particles using nanoSIMS provides fundamental compositional data about newly produced viruses, including specific information regarding the source and transfer of recently assimilated carbon and nitrogen by host cells during viral infection and lysis. Here we discuss the development and optimization of Viral-BONCAT and nanoSIMS and demonstrate their potential for marine microbial ecology research using three diverse bacterial and algal host-virus model systems, representing a range in viral particle sizes and metabolic capabilities. We further demonstrate the use of BONCAT in natural field populations for assessing new virus production in a pilot study using surface water collected off of the coast of Southern California.

Table 3. Percentage of BONCAT positive viral-like particles and corresponding *R:G* ratios from HPG incubation experiments with coastal seawater.

Treatment	% HPG-labelled	Viral particles analysed	Mean *R:G*
Positive HPG 48-h A	86.4 ± 0.7	32 404	0.21
Positive HPG 48-h B	85.8 ± 0.7	27 928	0.20
Positive HPG 72-h A	72.0 ± 0.9	26 477	0.16
Positive HPG 72-h B	85.4 ± 0.8	31 334	0.19
Negative Control	n/a	19 884	0.11
Negative Control	n/a	19 097	0.10

Percent labelled is given as the average ± 95% confidence interval.

Tracking elemental exchanges between viruses and their hosts via NanoSIMS

Over the past 15 years, the use of secondary ion mass spectrometry (SIMS and nanoSIMS) for measuring the stable isotope composition of microbial cells from environmental samples has become a valuable tool for assessing

Table 4. Comparison of Viral BONCAT estimate of virus turnover in coastal seawater with published estimates of turnover and viral production rates using different methods.

Viral production rates (viruses ml^{-1} day^{-1})	Viral turnover (days)	Geographical location	Method	Citation
16.4×10^6	1.5 days	Southern California, nearshore	BONCAT	This study
$12–230 \times 10^9$	0.5–3.9 days	Southern California Bight, nearshore	Incorporation of radiolabelled substrate	Steward and colleagues (1992b)
$0–2.8 \times 10^9$	8.9–30 days	Southern California Bight, offshore	Incorporation of radiolabelled substrate	Steward and colleagues (1992b)
$2.8–28 \times 10^6$	1–2 days	Southern California region	Fluorescently labelled viruses as tracers	Noble and Fuhrman (2000)
5.3–43 $x10^6$	5.1–27.8 days	Discovery Passage and Straight of Georgia (British Columbia, Canada)	Dilution technique	Wilhem and colleagues (2002)
$4.8–5.9 \times 10^7$	n/a	Chesapeake and Delaware Bays	Tangential Flow diafiltration dilution method	Winget and colleagues (2005)
$0.08–1.7 \times 10^6$	n/a	North Water	Frequency of visibly infected cells	Middleboe and colleagues (2002)
0.68 $–15.6 \times 10^8$	n/a	Coastal Bay, Norway	Viral decay rates	Heldal and Bratbak (1991)

the ecophysiology and specific roles of microorganisms in biogeochemical cycles (e.g., Orphan *et al.*, 2001; Cliff *et al.*, 2002; Musat *et al.*, 2008; Dekas *et al.*, 2009; Woebken *et al.*, 2012; Eichner *et al.*, 2017). To date, nanoSIMS-facilitated research in microbial ecology has focused on the analysis of bacteria, archaea and microeukaryotes. However, the use of high-resolution secondary ion imaging for analysing the isotope composition of environmentally relevant nanometer scale viruses has not been developed. Given that individual viral particles are near the 50 nm resolution limit of the nanoSIMS and the isotopic analysis of these nanometer-sized particles introduces a number of analytical challenges, we initially assessed whether the small size and C and N content within individual viruses could be detected by nanoscale secondary ion imaging with cesium. Additionally, we assessed whether the secondary ion yield from viruses was sufficient for detecting stable isotope ^{13}C and ^{15}N enrichment after growth of the host cells with ^{13}C and ^{15}N-labelled substrates.

Using two well-defined model photosynthetic eukaryotic (*E. huxleyi*) and cyanobacterial (*Synechococcus sp.* WH8101) hosts and their viruses (EhV207, ~200 nm capsid diameter; Syn1, ~80 nm capsid diameter), we demonstrated the ability to not only resolve viral particles using nanoscale secondary ion imaging, but also successfully measure ^{13}C and ^{15}N enrichment in individual viral particles after host lysis. Initial tests were based on host cells grown for multiple generations in the presence of ^{13}C-bicarbonate and a nitrogen source (either ^{15}N-ammonium for *Synechococcus sp.* WH8101 or ^{15}N-nitrate for *E. huxleyi*) followed by infection and viral particle recovery after lysis. NanoSIMS analysis of EhV207 and Syn1 produced a detectable and stable ion yield and sufficient $^{12}C^-$, $^{13}C^-$, $^{12}C^{14}N^-$ and $^{12}C^{15}N^-$ ions for stable isotope ratio measurements from individual viral particles (Figs. 2 and 4). By increasing the number of cycles and length of analysis time for each frame (i.e., dwell time), combined with the use of isotopically enriched host cells, we obtained sufficient precision to reliably differentiate ^{13}C and ^{15}N-enriched viral particles above the negative controls and background. Merging the data across individual frames increased the total ion counts for individual viral particles and reduced the error around each estimate (Supporting Information Fig. S3 and Appendix S1). Alternative analytical approaches to increase the secondary ion yield by increasing the intensity of the $Cs+$ primary ion beam current resulted in rapid sputtering and loss of these submicron-sized particles (see Supporting Information Appendix S1 for additional details).

The degree of variability and statistical uncertainty in the ^{13}C and ^{15}N nanoSIMS measurements was related to particle size, with greater variability in the measured ^{13}C and ^{15}N enrichment for the 80 and 200 nm viral particles (both within and across viral ROIs) relative to their larger host cells. Additionally, there was greater variability in the measured ^{13}C and ^{15}N for the smaller Syn1 viruses relative to EhV207 viruses (Figs. 2–4). These observations are consistent with our expectations based on the counting statistics. Incorporating this variability as propagated error (1σ) around each estimate translates to approximately 1–3 atom % uncertainty in the fractional C and N abundance measurements for individual viral particles. While nanoSIMS analysis can likely be extended to analyse viruses smaller than Syn1, the error around individual particle measurements will increase as the total ion counts per

virus target decreases. Despite the inherent uncertainty in the nanoSIMS stable isotope analysis, this method is still able to reliably differentiate ^{13}C and ^{15}N enriched viral particles after labelling of host cells from control populations of unlabelled viruses and, as discussed below, is also capable of resolving the proportion of enriched viruses from the total viral population from short term stable isotope probing experiments.

Overall, these culture-based experiments demonstrate that it is possible to measure ^{15}N or ^{13}C enrichment in viral particles above natural abundance values. Due to the low C and N ion yield per particle, however, also it is important to note that the uncertainty surrounding measurements of individual viral particles by nanoSIMS is large and complicates interpretation of the specific level of carbon or nitrogen enrichment. The absolute level of enrichment for an individual nanometer scale viral particle is confounded by high error from counting statistics and may also be influenced by inherent variability in the host ^{13}C or ^{15}N enrichment associated with growth rate differences and/or temporal lags between $^{13}C/^{15}N$-substrate uptake and viral lysis events. Therefore, the power of the nanoSIMS stable isotope tracer experiments is in obtaining quantitative estimates for the proportion of viruses that have been produced directly or indirectly from primary productivity (i.e., from infection of active autotrophic host cells) or from host organisms metabolizing a specific nutrient (e.g., nitrogen) or carbon source out of the total viral population recovered from the environment, rather than providing a direct comparison of the magnitude of enrichment levels between host microorganisms and virus.

The initial nanoSIMS lab experiments using fully ^{13}C and ^{15}N labelled host cells were valuable for our initial development and testing of this method. However, to track viral-host dynamics in naturally occurring communities using stable isotope probing, pre-enrichment of environmental host cells over many generations is not feasible. As such, we also tested the sensitivity of nanoSIMS to detect ^{15}N transfer between the *Synechococcus sp*. host and Syn1 after short (24-h) incubation times with ^{13}C-bicarbonate and ^{15}N-ammonium. These experiments verified the ability to resolve ^{13}C and ^{15}N enrichment within the 80 nm Syn1 particles after a short-term incubation experiment. Notably, the level of ^{15}N-enrichment of Syn1 (64 at%) was offset from values measured in the host Synechococcus (19 at%), a phenomenon that was not observed in the acclimated cultures grown for multiple generations in the presence of the isotope label (Fig. 2). The reason for this offset is not understood at this time. However one possible explanation is that the host microorganisms still retained a significant fraction of 'older' unlabelled biomass resulting in partial enrichment of the host after the 24 h incubation, whereas the viral particles produced after infection at the 24-h mark are comprised heavily of newly synthesized macromolecules synthesized during the incubation, enriched in the isotopically labelled substrate. Alternatively, this difference might also be explained by the offset in timing between the measurement of the host cells (subsample collected just prior to infection) and viruses recovered after host lysis. It is possible that over the 3-day infection period, the *Synechococcus* cells continued to assimilate additional ^{15}N prior to cell lysis, resulting in additional ^{15}N enrichment of the host. This temporal offset between host cells and virus is unavoidable in field measurements, as host cells can no longer be measured after lytic infection.

Despite the caveats associated with the stable isotope labelling approach, the results from our experiments demonstrate the ability to combine stable isotope probing with nanoSIMS for quantifying the fraction of ^{13}C or ^{15}N enriched viruses produced after infecting metabolically active hosts following assimilation of a specific isotopically labelled substrate. Coupled with ^{13}C-bicarbonate or different forms of ^{15}N-labelled nitrogen not only allows for the quantification of newly produced viral particles, but also offers a mechanism for directly linking viruses with the cycling of specific carbon and nitrogen substrates in the environment. This includes assessing the proportion of newly fixed carbon in autotrophic hosts that is shunted into the free viral fraction over time. The differentiation of isotopically enriched viruses from unlabelled viral particles during short term SIP experiments indicates that tracking the dynamics of substrate assimilation by environmental host microorganisms and associated viral production should be possible in the field.

Estimating viral production using Viral BONCAT

Accurate estimates of viral production in the ocean are critical for determining the influence of viral lysis on phytoplankton and bacterial mortality. A variety of methods have been employed to estimate viral production; these include, but are not limited to the incorporation of radiolabelled substrates into viral DNA (e.g., ^{3}H-thymidine or ^{32}P; Steward *et al*., 1992a,b; Fuhrman and Noble, 1995), TEM-based observations of visibly infected cells (e.g., Proctor *et al*., 1993; Steward *et al*., 1996), quantifying viral decay rates (e.g., Heldal and Bratbak, 1991; Bratbak *et al*., 1992), using fluorescently labelled viruses as tracers (e.g., Noble and Fuhrman, 2000; Ohno *et al*., 2012), and virus reduction approaches (e.g., Wilhelm *et al*., 2002; Helton *et al*., 2005; Winget *et al*., 2005; Weinbauer *et al*., 2010).

The viral-BONCAT and nanoSIMS methods developed in this work complement these earlier approaches while also providing additional information about viral production in ocean systems, either through linking viruses to specific host metabolisms using stable isotope labelling or by concomitant protein tagging of active viruses and their

corresponding host cells. The aforementioned stable isotope analysis of single viral particles by nanoSIMS provides quantitative, compositional data about the proportion of newly synthesized viruses and specific elemental exchanges between hosts, viruses, and the dissolved organic carbon/nitrogen pools in the ocean. However, due to the specialized instrumentation and detailed sample preparation, this method is inherently lower throughput and time consuming with large sample sets (Table 1). Fluorescence based methods such as the general protein-targeted Viral-BONCAT are comparatively inexpensive and easy to employ with minimal sample manipulation and experimental set up. Nucleic-acid based fluorescence staining of viruses is widely used in microbial ecology studies to visualize and count populations (e.g., Sherr *et al*., 1987; Noble and Fuhrman, 1998; Hennes *et al*., 1995; Zhang *et al*., 2010; Ohno *et al*., 2012; Allers *et al*., 2013). By targeting proteins rather than nucleic acids, Viral-BONCAT potentially targets a broader range of viruses, such as single stranded RNA/DNA viruses, which are currently missed with SYBR staining methods, but may represent a large proportion of the viral assemblage in the surface ocean (Steward *et al*., 2013; Roux *et al*., 2016b). As such, assuming that microbial hosts in the system under investigation actively incorporate HPG and transfer the modified methionine and/or proteins to viruses with enough HPG to generate a fluorescence signal above background, this approach should serve as a powerful complement to established methods of virus quantification and production measurements. See Supporting Information Appendix S4 for additional details on methodological considerations for measuring viral activity via Viral-BONCAT.

The Viral-BONCAT method was successfully developed and optimized using two cultured viral-host systems: the heterotrophic, bacterium *E. coli* and its 50 nm phage T7; and the photosynthetic eukaryote *E. huxleyi* and its ~200 nm virus EhV207. Similar to that of bacteria and archaea (Hatzenpichler *et al*., 2014; Samo *et al*., 2014), viral methionine content (at least for T7, Syn1 and EhV) is about 3% of the total amino acid pool (Supporting Information Table S1). Incorporation of host-derived HPG-labelled amino acids (or newly synthesized proteins) into viruses was distinguishable from BONCAT negative viral controls based on the *R:G* fluorescence ratio (Figs. 5 and 6). Our hypothesis, based on lytic culture dynamics, assumed that 100% of the viruses would become HPG labelled if their host was HPG-labelled. A small fraction of unlabelled viruses were initially added to each culture as infection inoculum, accounting for only ~1% of the total virus population after host lysis. The final estimates for the percent of newly synthesized viruses in the T7 (98%–99%) and EhV (87%–94%) Viral-BONCAT experiments are consistent with this prediction. Interestingly, about 5%–10% of the EhV viruses recovered at the end of the experiment remained unlabelled based on *R:G* ratios. Further work is needed to confirm the difference between *E. huxleyi* and *E. coli* viral production. Given the more nuanced, 'animal-like' infection phase dynamics of the *E. huxleyi*-EhV system (Mackinder *et al*., 2009; Grimsley, 2012), it is conceivable the BONCAT-negative particles may have been associated with an early 'chronic' phase of infection with viruses released by budding prior to active assimilation of HPG by hosts. This type of budding behaviour is not observed in the cyanobacterial virus model system.

The experimental BONCAT data from cultured virus-host systems (Figs. 5 and 6) and predictions from the sensitivity model (Figs. 7; Supporting Information Figs. S7 and S8) identified three main factors that influence the ability to quantify viral production using this method. These include: the number of methionine substitutions (n_{subs}) per virus, the magnitude of the shift in *R:G* ratio per substitution (*d*RG) and the percentage of the viral assemblage actively turning over (% active). These parameters were modelled as discrete values to provide benchmarks for our sensitivity analysis and data interpretation. Further tests of Viral-BONCAT with other virus-host model systems will enable better characterization of the variability in the number of substitutions and the impact of each substitution (n_{sub}) on the *R:G* ratio (*d*RG).

As a pilot study, we demonstrated the use of Viral-BONCAT with coastal seawater to detect BONCAT positive viral-like particles within a mixed community and estimate viral production rates in the field (Fig. 8). Unlike our model culture studies, the methionine substitution rate and the *d*RG is expected to vary among the diverse viral assemblages in environmental samples. Assuming all newly synthesized viral particles become HPG-labelled after lysing actively growing host cells, the relative proportion of HPG labelled *vs*. unlabelled viral particles provides a direct quantification of the number of newly synthesized viral particles produced over a given time period. Furthermore, if the decay rate is similar between HPG-labelled and unlabelled viral particles, comparing the number of HPG-labelled viruses relative to total viruses across two time points enables an estimation of net viral production rates (e.g., production-decay). Using probability statistics (as was done with the culture model systems), we were able to extract the number of fluorescently labelled viruses that were significantly greater than the unlabelled control and calculate viral production rates within the microbial community in surface waters collected off the Scripps Pier off of La Jolla, CA. However, viral production rate estimates are difficult to compare because they inherently depend on the concentration of viruses present in the sample; therefore, viral turnover is more amenable to comparisons across studies as it focuses on the relative proportion of the total viral assemblage, rather than an absolute concentration.

The estimated viral turnover from this experiment was 1.5 days, consistent with previous measurements in near shore southern California regions (Steward *et al.*, 1992b; Noble and Fuhrman, 2000).

This preliminary field study demonstrates the suitability of Viral-BONCAT for estimating viral production in a mixed or natural community. Focused, comparative studies are still needed to determine the best time-scales over which to sample and the frequency at which HPG should be added to the incubations. Shorter incubation times could provide hourly production rates, but the experimental time-scales need to allow for adequate turnover of the viral population (>25%) and long enough to ensure newly synthesized viral particles have sufficient HPG incorporation (>1 methionine substitution). The concentration of bioavailable environmental methionine relative to the amount of added HPG will also be important to consider as this ratio has been shown to influence HPG uptake (Samo *et al.*, 2014). In environments where cells are very active, continuous HPG additions may be needed to obtain sufficient labelling of the host populations (and viral particles) over time. This could be one plausible explanation for why we observed a reduction in the percentage of HPG-labelled viral particles between 48 and 72 h. Another possibility is that the host cells, from which those viruses were produced, did not take up HPG; HPG incorporation by the host is a prerequisite for Viral-BONCAT. Notably, active HPG assimilation has been demonstrated in diverse archaea, bacteria and microeukaryotes and in environmental samples (Hatzenpichler *et al.*, 2015; 2016; Samo *et al.*, 2014; Babin *et al.*, 2016, this study). Likewise, even microorganisms classified as obligate photo- or chemolithoautotrophs have been shown to actively assimilate amino acids from the environment (e.g., Ouverney and Fuhrman, 2000). Additional studies to test the applicability of this method in different environments as well as parallel methodological comparisons of virus production estimates using more standard approaches (e.g., virus reduction) are also needed. Overall, this technique advances our ability to assess the activity of viruses in the environment and offers an independent and direct approach to quantify viral production with minor sample manipulation and no dependency on conversion factors.

Future directions and implications for understanding viral-host interactions in the ocean

Our current understanding of the biogeochemical impact of marine viruses is limited by our ability to measure exchanges of nutrients and carbon between viruses and their environment. Direct efforts to quantify the influence of the 'viral shunt' are rare, with most studies indirectly estimating viral turnover rates and elemental release. The lack of straightforward and reliable approaches for estimating viral production and rates of viral mortality on phytoplankton and bacteria in the ocean remains one of the biggest obstacles for incorporating viral-mediated processes into global models of nutrient and energy cycling. Furthermore, tracing the fate of newly fixed carbon and nitrogen into different components of microbial food webs (e.g., phytoplankton, grazers, viruses and dissolved organic matter) is of great interest for understanding the direction, rates and magnitude of energy flow in marine ecosystems. The combination of measuring the fate of pathway specific stable isotope labels via nanoSIMS and general viral production by fluorescence via Viral BONCAT now enables the direct quantification of specific sources of C and N moving through the viral pool. The use of Viral-BONCAT provides a relatively inexpensive and rapid assessment of the fraction of free virioplankton that were recently involved lysing an active host cell. Coupled with incubations amended with different sources of ^{13}C-labelled carbon or ^{15}N-labelled nitrogen provides a mechanism for directly quantifying the proportion of active virioplankton that are involved in mediating the turnover of newly fixed carbon and nitrogen (via photosynthesis, chemosynthesis, diazotrophy, ammonium, or nitrate assimilation) relative to viruses involved in the lysis of heterotrophs over many different temporal and spatial scales. Future work will expand the use of stable isotope tracers beyond those used in this study (bicarbonate, nitrate and ammonium) to directly quantify the proportion of active virioplankton involved in mediating the turnover of carbon, nitrogen and potentially sulfur substrates in the surface oceans, mesopelagic or even more complex sediments and soils. Additional avenues could include creating isotopically labelled viral particles and trace the movement of enriched C and N from viruses into phytoplankton, grazers, heterotrophic bacteria and dissolved organic matter. Coupling these activity- and isotope-based techniques with other powerful microbial ecology methods (e.g., flow cytometry cell sorting, genomics, proteomics) opens up exciting possibilities for viral ecology studies (Brussaard *et al.*, 2016).

Another potential application of Viral-BONCAT is to identify specific viral proteins produced during the lytic infection. Combining BONCAT with proteomics (e.g., Babin *et al.*, 2016; Bagert, 2016) provides information about newly synthesized viral proteins and potentially changes in protein expression over time in tandem with taxonomic information (e.g., capsid protein sequences) in the context of their natural environment. HPG substitution into specific proteins was confirmed by mass spectrometry from experiments using BONCAT-positive T7 and EhV viruses, with many of the detected HPG-labelled proteins involved in procapsid and capsid formation and DNA packaging (Table 2). Moniruzzaman and colleagues (2017) recently demonstrated the utility of the Major Capsid Protein (MCP) as a marker for infection dynamics and diversity in natural

populations. Therefore, tracking changes in HPG-labelled viral proteins over time in other cultures and extending this to natural environments (e.g., tracking HGP incorporation into MCP) provides us an exciting opportunity to characterize infection dynamics at the protein level.

Proteomics coupled with BONCAT can also be used to better characterize viral diversity and biogeography, an important and growing area of exploration in the field of marine virology (Breitbart *et al*., 2002; 2004; Brum *et al*., 2015; Hurwitz *et al*., 2015; Roux *et al*., 2016a). One major advantage of protein targeted Viral BONCAT is that, unlike currently available fluorescent nucleic acid stains that are limited to double stranded DNA viruses, BONCAT has the potential to also label single-stranded DNA and RNA viruses (Steward *et al*., 2013; Roux *et al*., 2016b). Successful sorting of HPG-labelled viruses (via fluorescence signal) prior to metagenomic or metatranscriptomic analysis would allow for a comparison of active virus populations (e.g., FCM sorted viral genomes) among the total viral pool (e.g., bulk viral metagenomes) and help to highlight factors that influence active viral communities over space and time and enhance viral success in the ocean (Angly *et al*., 2006; Breitbart, 2012).

Experimental procedures

Viral-host cultures and isotope experimental incubations

Emiliania huxleyi (CCMP strain 374) and its lytic virus EhV 207 (~200 nm capsid) was used as a eukaryotic host-virus model system. *E. huxleyi* was obtained from the National Center for Marine Algae and Microbiota, and its virus was isolated in 2001 from the English Channel (Schroeder *et al*., 2002) and kindly provided by M. Allen (Plymouth Marine Lab). *E. huxleyi* was grown on an enriched artificial seawater media (ESAW without silicate; Harrison *et al*., 1980). Batch cultures were maintained at 18°C on a 14:10 light:dark cycle at ~150 μmol photons m^{-2} s^{-1}. EhV207 was propagated by infecting cultures grown in f/2 minus silicon. Upon complete host lysis, viral lysates were filtered through a 0.45-μm syringe filter to remove cellular debris and stored at 4°C in the dark. Viral abundance was determined using SYBR Gold (Life Technologies) and flow cytometry (Brussaard, 2004b). *Synechococcus sp*. (strain WH 8101, Waterbury *et al*., 1986) with lytic virus Syn1 (~80 nm capsid) was used as a cyanobacterial host-virus model system. *Synechococcus* WH8101 culture was kindly provided by Dr. Gabrielle Rocap (University of Washington, School Oceanography). Prior to the experiments, the culture was acclimated to growth on 100% artificial seawater Amp1 media (Rippka, 1988) using a 14:10 light:dark cycle. The Amp1 was prepared as indicated by Moore and colleagues (2007). Syn1 virus was propagated using unlabelled batch cultures of *Synechococcus* WH8101 grown on a 50/50 mix of Amp1 and SN (Waterbury and Willey, 1988) media without isotopically labelled carbon or nitrogen under low light conditions (20 μmol photons m^{-2} s^{-1}).

Single isotope-label virus enrichment experiments were done with hosts grown on either (i) ^{13}C-labelled media, (ii) ^{15}N-labelled media or (iii) an unlabelled control. *Synechococcus sp*. was grown on Amp1 media with either (i) 6 mM ^{13}C-sodium bicarbonate ($NaH^{13}CO_3$; 50% label) and 400 μM unlabelled ammonia (NH_4) (Exp. 1), (ii) 400 μM $^{15}NH_4$ (100% label) and 6 mM unlabelled-$NaHCO_3$ (Exps. 2 and 3), or (iii) 400 μM unlabelled-NH_4 and 6 mM unlabelled-$NaHCO_3$. Unlabelled cultures were used to inoculate new labelled-cultures for virus enrichment experiments. These newly inoculated cultures were then passed two times into fresh isotopically labelled media (splitting the culture 1:5 into new media after 7 and 8 days for Exps. 1 and 3 respectively). After the second transfer, exponentially growing host cells were sampled to provide the level of host labelling prior to infection. Host cells were fixed with glutaraldehyde (0.5% final concentration) at room temperature for 15 min, flash frozen and stored at −80°C. Syn1 was then added at a multiplicity of infection (MOI) of ~5 for 24 h. After 24 h, fresh media (with the appropriate label) was used to dilute the culture approximately 1:3. Cells were lysed to completion (approximately 7 days) at which point viruses were collected. Virus samples were filtered through a 0.2-μm filter, fixed with glutaraldehyde (0.5% final concentration) for 15 min at room temperature, flash frozen and stored at −80°C until further analysis.

An additional short-term isotope enrichment experiment was performed with *Synechococcus sp*. and Syn1 to determine if isotope transfer could be detected in the viral particles after pulsing a labelled substrate rather than growing the cultures for many generations on labelled substrates. Cultures grown in unlabelled Amp1 media were transferred to media with 400 μM $^{15}NH_4$ (100% label) at a 1:5 dilution and incubated for 24 h. After 24 h, host cells were sampled and viruses were added at an MOI of 1.The culture was lysed to completion (approximately 5 days) at which point viral samples were collected as described above.

E. huxleyi CCMP 374 was grown in ESAW media with either (i) 1.2 mM $NaH^{13}CO_3$ (100% label) and 553 μM unlabelled-nitrate (NO_3) (Exp. 1), (ii) 553 μM $^{15}NO_3$ (100% label) and 1.2 mM unlabelled-$NaHCO_3$ (Exp. 2) or (iii) 553 μM unlabelled-NO_3,and 1.2 mM unlabelled-$NaHCO_3$. *E. huxleyi* cultures were grown on labelled media for a minimum of 10 generations prior to the start of virus enrichment experiments. At the start of each experiment, exponentially growing cultures were harvested by centrifugation (3000 × g, 10 min) to provide the level of host labelling prior to infecting with EhV207 at an MOI of 5. EhV207 viruses were added directly to the culture with no additional transfers or dilutions. Upon host lysis (~ 3 d), viral lysates were collected by filtering through a 0.45-μm syringe filter, fixed in 0.5% glutaraldehyde for 15 min at 4°C, then flash frozen in liquid nitrogen and stored at −80°C until further analysis. A dual-labelled viral enrichment experiment (Experiment 3) was set up similar to single-label experiments with the exception that *E. huxleyi* was grown in ESAW media containing both 1.2 mM $NaH^{13}CO_3$ (100% label) and 553 μM $^{15}NO_3$ (100% label) for ~6 months prior to the start of virus enrichment experiments.

Adsorption control experiments were performed with *E. huxleyi* to determine the influence of fixation on nitrogen adsorption to the outside of the cell. *E. huxleyi* was grown in unlabelled ESAW. Cells were harvested and fixed in glutaraldehyde (2% final concentration) at 4°C for 15 min. Cells were washed 3 times with unlabelled media and resuspended in

either $^{15}NO_3$ or $^{15}NH_4$ labelled media and stored at 4°C for 2 days prior to being stored at −80°C.

NanoSIMS sample preparation and microscopy

Aliquots (10–20 μl) of fixed virus particles and host cells were spotted separately onto custom-cut silicon wafers (WSI08–1108001, Active Business Company GmbH). Prior to spotting the samples, fiduciary marks were added to the silicon wafers using a laser microdissection (Leica LMD7000) microscope. These marks were used as reference points to locate and precisely correlate fluorescence microscopy and nanoSIMS images. After viral particles and host cells were deposited on the surface of the silicon wafers, samples were rinsed with 0.02-μm filtered water and air-dried. Viruses and hosts were stained using SYBR gold (Life Technologies, 10× final concentration; 1:1000 dilution of 10 000× stock) for 15 min in the dark, washed with 0.02-μm filtered water and air-dried. Wafers were subsequently imaged by fluorescence microscopy on the LMD microscope using a FITC filter set and a 60X (for hosts cells) or 150X (for viral particles) dry objective. *E. huxleyi*, *Synechococcus sp.*, and EhV were large enough for imaging with the dry objective, but the fluorescence was not bright enough to reliably image the smaller Syn1 viral particles. Instead, Syn1 was imaged using a 100X oil immersion objective on an upright epifluorescence microscope (Olympus BX51) with FITC filter set. Water soluble vectashield (Vector Laboratories) was used as anti-fade mounting solution and subsequently removed with 0.02-μm filtered water with water prior to nanoSIMS analysis. Gold nanoparticles (100 nm, OD 1, stabilized suspension in 0.1 mM PBS; Sigma-Aldrich) were tested as possible fiduciary markers with Syn1 (Exp. 3) to assist with locating pre-imaged viruses for nanoSIMS analysis. 1 μl of gold bead suspension was mixed with the sample directly on the wafer. Gold beads were mapped with both reflected light filter and using a 100X oil immersion objective in the same regions the viral particles were imaged.

NanoSIMS instrument conditions and analysis

All samples were analysed with a CAMECA NanoSIMS 50L (CAMECA, Gennevilliers, France) housed in the Division of Geological and Planetary Sciences at the California Institute of Technology. LMD marked and fluorescence microscopy mapped sample regions were located using the NanoSIMS CCD camera. Viruses were analysed using a ~0.8–1 pA primary Cs^+ beam current with a nominal spot size of ~100 nm without pre-sputtering. Host cells were first pre-sputtered with 30–70 pA primary Cs^+ beam current for 1 frame (approximately 11 min) and then analysed using a 1 pA primary Cs^+ beam current. Five masses were collected in parallel ($^{12}C-$, $^{13}C-$, $^{14}N^{12}C-$, $^{15}N^{12}C-$, $^{28}Si-$) using electron multipliers (EMs). During two runs, $^{12}C^{13}C-$ and $^{12}C_2-$ were collected instead of $^{12}C-$ and $^{13}C-$. $^{197}Au-$ was also collected when testing the use of gold beads with nanoSIMS. For all analyses, the beam was rastered over a square region (ranging from 3 × 3 μm to 10 × 10 μm for viruses and 10 × 10 μm to 20 × 20 μm for host cells) for approximately 11 min per analytical plane/frame. At least 15 and 10 frames were collected per analysis for virus and host, respectively. All ion images were recorded at 256 × 256 pixel resolution with a dwell time of 10 ms/pixel. Mass calibration was done every ~30 min for all ions.

NanoSIMS data analysis

Raw data from ion images were processed using the open-source MATLAB plugin Look@NanoSIMS (LANS; Polerecky *et al.*, 2012). Ion images from multiple frames were corrected for EM dead time and quasi-simultaneous arrival (QSA) effect and then aligned and accumulated. In most cases $^{14}N^{12}C-$ was used to align images. However, for the smallest viral particles (Syn1) aligning images across multiple planes was sometimes difficult due to low count rates and $^{197}Au-$ was used for aligning images whenever gold nanoparticles were included in the wafer preparation (Exp. 3). Regions of interest (ROIs) were drawn using either the $^{14}N^{12}C-$ or $^{15}N^{12}C-$ ion image to identify the outline of the viral particle or host cell. All ROIs represent individual viral particles or individual host cells.

Isotope calculations of viruses and their hosts were based on raw ion counts exported from LANS (Polerecky *et al.*, 2012). All calculations and data processing was performed in R (R Development Core Team, 2013) using the package *lans2r*. When the molecular ions $^{13}C^{12}C$ and $^{12}C_2$ were collected, the $^{13}C/^{12}C$ ratio was calculated as half of the R_{sample} from the raw ion counts of $^{13}C^{12}C$ and $^{12}C_2$. Counting error was propagated to the isotope ratio by standard error propagation based on a Poisson distribution (see Supporting Information Appendix S1 for details). Instrumental isotope fractionation of the nanoSIMS was determined and corrected for within each run by comparing the NanoSIMS acquired $^{13}C/^{12}C$ and $^{15}N/^{14}N$ ratios for all combined natural abundance (unlabelled) particles analysed (virus and host) against the expected circum-natural abundance ratios ($^{13}C/^{12}C = 0.011$; $^{15}N/^{14}N = 0.0036$; Supporting Information Fig. S1, Appendix S1). Due to the high isotope enrichments associated with tracer experiments, it is more intuitive to compare fractional abundances rather than isotope ratios. Ion ratios were converted to fractional abundance using the relationship $F_{sample} = R_{sample}/(1 + R_{sample})$, where F is the fractional abundance and R is the ratio of either $^{13}C/^{12}C$ or $^{15}N/^{14}N$. Errors from counting statistics and instrumental mass fractionation were propagated for conversion to fractional abundance (see Supporting Information Appendix S1 for more details).

Viral BONCAT – experimental incubations, microscopy, digital image analysis and data analysis

Bioorthogonal non-canonical amino acid tagging (BONCAT) experiments were done with *Escherichia coli* K12 (kindly provided by D. Tirrell; Caltech) and T7 (kindly provided by R. Phillips; Caltech) as well as with *E. huxleyi* and EhV (described above). Incorporation of L-homopropargylglycine (HPG), a methionine analogue, into new protein has been previously demonstrated for *E. coli* (Beatty *et al.*, 2005; Wang *et al.*, 2008), but not for *E. huxleyi*.

E. coli K12 was grown at 37°C in M9 minimal medium: 0.5 g NaCl, 2.0 g of glucose, 1.0 g NH_4Cl, 12.8 g Na_2HPO_4 × 7 H_2O, 3.0 g KH_2PO_4, 492 mg $MgSO_4$ × 7 H_2O, 11 mg

$CaCl_2$, 100 mg thiamine per 1 l of deionized water. HPG (Click Chemistry Tools, L-homopropargylglycine resuspended in H_2O; 100 μM final concentration) was added to exponentially growing *E. coli* (OD600 = 0.3) and incubated for approximately one generation (OD600 = 0.6) prior to adding virus. A control treatment without HPG was run in parallel to the experimental treatment. Phage T7 was then added (MOI of 2) and the culture was lysed to completion. On host lysis, viral samples were filtered through a 0.2-μm filter to remove cell debris, fixed with paraformaldehyde (PFA; 2% final concentration) for 15 min at 4°C and stored in the −80°C until further analysis. For proteomics, 0.2-μm filtrate was concentrated using 100 kDA Amicon ultra centrifugal filter (EMD Millipore). Approximately 4 ml of culture was concentrated into 250–500 μl and frozen at −80°C until extraction and digestion.

For *E. huxleyi*, HPG (resuspended in DMSO; 100 μM final concentration) was added to an exponentially growing culture in unlabelled ESAW minus Si media and incubated under 14:10 LD dark cycle at 150 μmol photons m^{-2} s^{-1} for 24 h. A control treatment with an equivalent volume of DMSO was run in parallel to the experimental treatment. After 24 h, a subsample of host cells was harvested by centrifugation to examine the incorporation of HPG by the host. EhV207 (MOI of 5) and an additional pulse of HPG (100 μM final) were then added to the remaining culture. Upon host lysis, viral samples were filtered through a 0.45 μm filter, fixed with glutaraldehyde (0.5% final concentration) for 15 min at 4°C, flash frozen in liquid nitrogen and stored at −80°C until further analysis. For proteomics, 0.45-μm filtrate was concentrated using 100 kDA Amicon ultra centrifugal filter (EMD Millipore). Approximately 20 ml of culture was concentrated into 250–500 μl and frozen at −80°C until extraction and digestion.

An additional field experiment with HPG additions was performed with seawater collected from the Scripps Pier in La Jolla, California (32.87 N, 117.26 W). Surface waters were collected at 17:00 h on 9 October 2016 and stored in a polycarbonate carboy at 10°C until the experiment was started at 08:00 h on 10 October 2016. Seawater was placed into 250 ml incubation bottles. Treatment bottles (in replicate) were amended with 100 μM of HPG relative to negative controls (e.g., no HPG additions). Incubations were maintained at 18.7°C (October pier temperature average: https://tidesandcurrents.noaa.gov) under a 12 h:12 h light:dark cycle at 100 μmol m^{-2} s^{-1} of photosynthetically active radiation (PAR). Samples for time points T_0, T_{48} and T_{72} h were taken to quantify virus concentration and incorporation of HPG. For this initial field test, fast growing populations with lytic cycles ranging from 12–48 h were targeted. Therefore, sampling was delayed by 48 h in order for host cells to grow in the presence of HPG and viral lysis to occur. Viral concentration was determined using traditional epifluorescence microscopy methods (Noble and Fuhrman, 1998; Patel *et al.*, 2007). In short, glutaraldehyde fixed samples (1 ml) were gently filtered (0.5 mmHg) onto 0.02 μm Anodisc filters with HA backing filters, dried and stained for 15 min with SYBR Gold (0.25% final concentration). After staining, the filters were dried in the dark and mounted onto slides with 0.1% p-phenylenediamine anti-fade mounting solution. Samples for determining HPG incorporation into viruses were prepared differently to concentrate viruses from a larger volume of seawater and reduce background fluorescence for image analysis. Seawater samples (8 ml in duplicate) were concentrated using an Amicon Ultra Centrifugal filter (Millipore, 100 K, UFC810096) to approximately 30 μl following the manufacturer's recommendations (i.e., 4000 rcf for 15 min). Samples were fixed with glutaraldehyde (0.5% final concentration), flash frozen and stored at −80°C until further analysis.

Prior to the copper (I)-catalysed cycloaddition, or click reaction, all samples (cultured and natural seawater) were spotted (2–5 μl) directly onto Teflon printed glass slides (Electron Microscopy Sciences, PTFE Printed Slides), air-dried, rinsed with 0.02-μm filtered water and air-dried again. Samples were put through an ethanol dehydration series (50:50, 80:20, 96:4 v/v EtOH:H_2O) prior to incubation with freshly prepared click solution (4 μl of dye-premix [CuSO4, 0.1 mM; THPTA, 0.5 mM; TAMRA-azide fluorophore, 2 μM] was added to 245 μl of buffer solution [sodium ascorbate, 5 mM; aminoguanidine hydrochloride, 5 mM; 1X PBS]). Click solution (20 μl) was spotted onto the sample and incubated in a humid chamber (a sealed 50 ml falcon tube with water on tissue paper in the bottom) at room temperature in the dark for 30 min. Following incubation, the sample was washed with 1X PBS, water and 50:50 v/v EtOH:H_2O. Samples were counterstained for 15 min with SYBR Gold (0.25% final concentration), washed with water and air-dried.

Viral samples were analysed with an Olympus BX51 upright epifluorescence microscope using a 100X objective (UPLFLN 100X 1.3 NA). Digital images were captured with a QIClick 12bit CCD digital camera using two filter sets: a FITC filter set (excitation 480/40 nm; emission 535/50 nm) and a Cy3 filter set (excitation 545/30 nm; emission 620/60 nm). Incorporation of HPG by viruses was quantified from these digital images by measuring the fluorescence signal of the azide-containing TAMRA fluorophore (i.e., click signal in Cy3) relative to the fluorescence signal from the SYBR Gold (i.e., DNA signal in FITC) within individual viral particles using a custom Matlab analysis pipeline (see Supporting Information Appendix S2 for more details and link to analysis code). In short, FITC and Cy3 images were corrected for uneven background illumination (based on a disk structuring element) and aligned with one another. Regions of interest (ROIs) were selected by applying a signal threshold with a size cutoff to the FITC image. In fluorescence microscopy, the resolution (the minimum distance required to resolve two particles from one another – $R = \lambda/[2 \times \mathrm{NA}] = 0.184$ μm – set by the objective numerical aperture [N; UPLFLN 100× 1.3N] and the wavelength of light used [λ; 480 nm for FITC filter]) does not limit the ability to accurately count small fluorescently labelled objects as long as they are separated from one another by more than the resolution distance. The centroid of each fluorescent ROI can therefore be used to locate the ROI with nanometer precision, far beyond the resolution limits of the microscope (Churchman *et al.*, 2005; Yildiz and Selvin 2005; Waters 2009). Image analysis of non-clicked T7, Syn1 and EhV was used to confirm that individual viral particles (across a range of sizes; 50–200 nm) would be identified as ROIs based on their FITC signal from SYBR Gold DNA staining. Finally, green (FITC) and red (Cy3) fluorescence values were recorded for each ROI and data was normalized by image exposure time. Histograms of the red-to-green (*R:G*) ratios of individual viral particles (at least > 1000 particles per treatment) were used to visualize differences in the viral

populations from each experiment and/or treatment. A Wilcoxon Rank-Sum test was used to determine if the *R:G* ratio distributions between treatments with and without HPG were significantly different from one another. To quantify the number of newly synthesized viral particles and evaluate confidence intervals around our estimates, we coupled a rank-sum test with a bootstrap approach to determine the probability that a random sample drawn from the sample *R:G* distribution is greater than a random sample drawn from the negative control *R:G* distribution (see Supporting Information Appendix S2 for details and link to code). To assess under what conditions our theoretical approach accurately captures viral production (e.g., the percent of newly synthesized viral particles), we then tested our ability to determine the number of newly synthesized viruses from a simulated data set of T7 by this method. For the field data, viral production rates were calculated using the equations from Noble and Fuhrman (2000), but rather than track the disappearance of fluorescently labelled viruses, we essentially tracked the disappearance of unlabelled viruses as fluorescently labelled viruses were produced (see Supporting Information Appendix S2 for details). Viral turnover (days) was estimated by dividing the average number of viral particles by the virus production rate.

Proteomics

Protein was extracted from concentrated T7 and EhV in a 1:1 ratio with lysis buffer (200 mM Tris-HCl pH 8, 4% SDS) and a protease inhibitor (1 tablet for 10 ml of reaction) in a screw-cap tube. The sample was boiled for 15 min in water bath. Protein was quantified using Bradford Protein Assay (Bio-Rad Laboratories). A filter-aided sample preparation (FASP) procedure was used to clean (e.g., remove SDS) and digest proteins in preparation for proteomic analysis (Wiśniewski *et al.*, 2009). Eluted peptides were lyophilized, resuspended in 100 μl of 0.2% formic acid and desalted by HPLC with an Optimized Technologies C8 peptide Macrotrap (3 × 8 mm; 200 μg maximum capacity). Desalted peptides were then lyophilized and stored at −20°C until mass spectrometry analysis.

Liquid chromatography-mass spectrometry was carried out on a Q-Exactive HF Orbitrap mass spectrometer (Thermo Fisher Scientific, Bremen, Germany) in the Proteome Exploration Laboratory at the Beckman Institute at Caltech. For the LC-MS/MS experiments, samples were loaded onto a custom-packed column (ReproSil-Pur 120 $C18_{AQ}$ 1.9 μM; 50 μm internal diameter × 20 cm long). The column was enclosed in a column heater operating at 60°C. The peptides were separated with a 120 min elution gradient (0–40% solvent B) at a flow rate of 220 nl min^{-1}. The Orbitrap was operated in data-dependent acquisition mode to alternate automatically between a full scan (*m/z* 300–1700) and 12 subsequent HCD (higher energy collisional dissociation) MS/MS scans in the orbitrap.

Thermo raw files were processed and searched with MaxQuant (v. 1.5.3.30) (Cox and Mann, 2008; Cox *et al.*, 2011). For *E. coli*/T7 samples, all UniProt *E. coli* entries (4311 sequences) and all UniProt T7 entries (57 sequences) were searched along with a contaminant database containing proteins such as keratin and trypsin (247 sequences). For *E. huxleyi*/EhV207 samples, all UniProt *E. huxleyi* entries (35 700 sequences) and EhV207 entries (470 sequences) were searched along with the same contaminant database as used for the *E. coli* search. Trypsin was specified as the digestion enzyme with up to two missed cleavages allowed. Protein N-terminal acetylation (+42.0106), Met oxidation (+15.9949), Met->Aha conversion (–4.9863) and Met->Hpg conversion (–21.9877) were specified as variable modifications. Carbamidomethylation of cysteine (+57.0215) was specified as a fixed modification. Match between runs, LFQ and iBAQ were enabled. Precursor ion tolerance was 4.5 ppm after recalibration and fragment ion tolerance was 20 ppm. Additionally, a decoy database was constructed to determine the false discovery rate by reversing the target database. Using the decoy database, the protein, peptide and modified site level false discovery rates were set to be less than 1%.

Viral BONCAT sensitivity testing

The ability to detect newly synthesized viral particles via Viral BONCAT depends on the number of HPG substitutions per viral particle and the influence of an HPG substitution on the measured *R:G* ratio. By modelling variations in these parameters (based on knowledge from T7), we explored the sensitivity of Viral BONCAT to detect newly synthesized viral particles under different scenarios of viral activity (i.e., the fraction of the viral pool that is actively turning over or % active). The model is briefly described below, but additional details and links to download the code can be found in Supporting Information Appendix S2. The number of detected substitutions (n_{subs}) and the impact of an HPG substitution on the *R:G* ratio (*d*RG) were estimated from T7 data (12 and 0.0491 respectively). However, depending on where the substitution sites are located and the size of the viral proteome, these parameters may vary; therefore, we considered a range of values for each parameter. We simulated the production of new viruses by adding a random number of methionine substitutions (modelled with a binomial distribution each increasing the *R:G* fluorescence ratio by a specific amount) to a subset (x percent) of the negative control *R:G* ratios with a different number of particles in play. Using 1000 particles drawn from the T7 negative control distribution, we explored how the following conditions impacted the probability distributions of HPG-labelled particles: $n_{subs} = 1, 5, 12$; $dRG = 0.01, 0.03, 0.05$; % active = 5, 25, 50, 75, 100. In an effort to model the variability that individual substitutions may have on the actual changes in *R:G*, we also explored how percent variations in *d*RG (± % of the average *d*RG) for individual substitutions influenced the shape of the probability distributions for HPG-labelled viruses.

Acknowledgements

We thank K. Dawson and G. Chadwick for many insightful conversations regarding data interpretation and analysis and R. Hatzenpichler and B. Babin for useful discussions regarding BONCAT and click chemistry. We also thank J. Nissomov, F. Natale and J. Latham for their technical assistance with the *E. huxleyi*-EhV experiments as well as Jennifer Brum and Sarah Schwenck for help exploring the use of TEM microscopy for mapping Syn1 viral particles. This work was funded by the Gordon and Betty Moore Foundation through Grant GBMF3780 to VJO, GBMF3789 to KDB and GBMF3305 and

GBMF3790 to MBS as well as NSF Biological Oceanography awards to KT, KDB (OCE-1559179) and MBS (OCE-1536989). ALP was supported by an NSF OCE Postdoctoral Research Fellowship. The Caltech Proteome Exploration Laboratory is supported by the Gordon and Betty Moore Foundation through grant GBMF775, the Beckman Institute and NIH (S10OD020013).

References

Allers, E., Moraru, C., Duhaime, M.B., Beneze, E., Solonenko, N., and Barrero-Canosa, J. (2013) Single-cell and population level viral infection dynamics revealed by phageFISH, a method to visualize intracellular and free viruses. *Environ Microbiol* **15:** 2306–2318.

Angly, F.E., Felts, B., Breitbart, M., Salamon, P., Edwards, R.A., and Carlson, C. (2006) The marine viromes of four oceanic regions. *PLOS Biol* **4:** e368.

Babin, B.M., Bergkessel, M., and Sweredoski, M.J. (2016) SutA is a bacterial transcription factor expressed during slow growth in Pseudomonas aeruginosa. *Proc Natl Acad Sci USA* **113:** E597–E605.

Bagert, J.D. (2016) Time-resolved proteomic analysis of quorum sensing in Vibrio harveyi. *Chem Sci* **7:** 1797–1806. doi: 10.1039/c5sc03340c

Beatty, K.E., Xie, F., Wang, Q., and Tirrell, D.A. (2005) Selective dye-labeling of newly synthesized proteins in bacterial cells. *J Am Chem Soc* **127:** 14150–14151.

Bratbak, G., Heldal, M., Thingstad, T.F., Riemann, B., and Haslund, O.H. (1992) Incorporation of viruses into the budget of microbial C-transfer A first approach. *Mar Ecol Prog Ser* **83:** 273–280.

Breitbart, M. (2012) Marine viruses: truth or dare. *Annu Rev Marine Sci* **4:** 425–448.

Breitbart, M., Salamon, P., Andresen, B., Mahaffy, J.M., Segall, A.M., Mead, D., *et al.* (2002) Genomic analysis of uncultured marine viral communities. *Proc Natl Acad Sci USA* **99:** 14250–14255.

Breitbart, M., Miyake, J.H., and Rohwer, F. (2004) Global distribution of nearly identical phage-encoded DNA sequences. *FEMS Microbiol Let* **236:** 249–256.

Breitbart, M., Middelboe, M., and Rohwer, F. (2008) Marine viruses: community dynamics, diversity and impact on microbial processes. In *Microbial Ecology of the Oceans, Second Edition*. Kirchman, D.L. (ed). Hoboken, NJ: Wiley.

Brum, J.R., and Sullivan, M.B. (2015) Rising to the challenge: accelerated pace of discovery transforms marine virology. *Nat Rev Microbiol* **13:** 147–159.

Brum, J.R., Ignacio-Espinoza, J.C., Roux, S., Doulcier, G., Acinas, S. G., Alberti, A., *et al.* (2015) Patterns and ecological divers of ocean viral communities. *Science* **358:** 1261498.

Brussaard, C.P.D. (2004a) Viral control of phytoplankton populations - a review. *J Eukaryot Microbiol* **5:** 125–138.

Brussaard, C.P.D. (2004b) Optimization of procedures for counting viruses by flow cytometry. *Appl Environ Microbiol* **70:** 1506–1513.

Brussaard, C.P.D., Bidle, K.D., Pedrós-Alió, C., and Legrand, C. (2016) The interactive microbial ocean. *Nat Microbiol* **2:** 16255.

Churchman, L.S., Okten, Z., Rock, R.S., Dawson, J.F., and Spudich, J.A. (2005) Single molecule high-resolution colocalization of Cy3 and Cy5 attached to macromolecules measures intramolecular distances through time. *Proc Natl Acad Sci USA* **102:** 1419–1423.

Cox, J., and Mann, M. (2008) MaxQuant enables high peptide identification rates, individualized p.p.b.-range mass accuracies and proteome-wide protein quantification. *Nat Biotechnol* **26:** 1367–1372.

Cox, J., Neuhauser, N., Michalski, A., Scheltema, R.A., Olsen, J.V., and Mann, M. (2011) Andromeda: a peptide search engine integrated into the MaxQuant environment. *J Proteome Res* **10:** 1794–1805.

Dattagupta, S., Schaperdoth, I., Montanari, A., Mariani, S., Kita, N., Valley, J.W., *et al.* (2009) A novel symbioses between chemoautotrophic bacteria and freshwater cave amphipod. *ISME J* **3:** 935–943.

Dieterich, D.C., Link, A.J., Graumann, J., Tirrell, D.A., and Schuman, E.M. (2006) Selective identification of newly synthesized proteins in mammalian cells using bioorthogonal noncanonical amino acid tagging (BONCAT). *Proc Natl Acad Sci USA* **103:** 9482–9487.

Dekas, A.E., Poretsky, R.S., and Orphan, V.J. (2009) Deep-sea archaea fix and share nitrogen in methane-consuming microbial consortia. *Science* **326:** 422–426.

Edwards, R.A., McNair, K., Faust, K., *et al.* (2015) Computational approaches to predict bacteriophage-host relationships. *FEMS Microbiol Rev* **40:** 285–272.

Eichner, M.J., Klawonn, I., Wilson, S.T., Littmann, S., Whitehouse, M.J., Church, M.J., *et al.* (2017) Chemical microenvironments and single-cell carbon and nitrogen uptake in field-collected colonies of *Trichodesmium* under different pCO_2. *ISME J* **11:** 1305–1317.

Evans, C., and Wilson, W.H. (2008) Preferential grazing of *Oxyrrhis marina* on virus-infected Emiliania huxleyi. *Limnol Oceanogr* **53:** 2035–2040.

Fuhrman, J.A. (1999) Marine viruses and their biogeochemical and ecological effects. *Nature* **399:** 541–548.

Fuhrman, J.A., and Noble, R.T. (1995) Viruses and protists cause similar bacterial mortality in coastal seawater. *Limnol Oceanogr* **40:** 1236–1242.

Frada, M.J., Schatz, D., Farstey, V., Ossolinski, J.E., Sabanay, H., Ben-Dor, S., *et al.* (2014) Zooplankton may serve as transmission vectors for viruses infecting algal blooms in the ocean. *Curr Biol* **24:** 2592–2597.

Grimsley, N.H., Thomas, R., Kegel, J.U., *et al.* (2012) Genomics of Algal Host-Virus Interactions. In *Genomic Insights into the Biology of Algae, Advances in Botanical Research*, Vol. 64. Piganeau, G., (ed). San Diego, CA: Academic Press, pp 343–381.

Guidi, L., Chaffron, S., Bittner, L., Eveillard, D., Larhlimi, A., Roux, S., *et al.* (2016) Plankton networks driving carbon export in the oligotrophic ocean. *Nature* **532:** 465–470.

Hara, S., Terauchi, K., and Koike, I. (1991) Abundance of viruses in marine waters: assessment by epifluorescence and transmission electron microscopy. *Appl Environ Microbiol* **57:** 2731–2734.

Harrison, P.J., Waters, R.E., and Taylor, F.J.R. (1980) A broad spectrum artificial medium for coastal and open ocean phytoplankton. *J Phycol* **16:** 8–35.

Hatzenpichler, R., Scheller, S., Tavormina, P.L., Babin, B.M., Tirrell, D.A., Orphan, V.J., (2014) In situ visualization of newly synthesized proteins in environmental microbes

using amino acid tagging and click chemistry. *Environ Microbiol* **16:** 2568–2590.

Hatzenpichler, R., and Orphan, V.J., (2015) Detection of protein-synthesizing microorganisms in the environment via bioorthogonal non-canonical amino acid tagging (BONCAT). In Hydrocarbon and Lipid Microbiology Protocols, Vol. 7: Single-cell and single-molecule methods. Springer Protocols Handbooks. doi:10.1007/8623_2015_61.

Hatzenpichler, R., Connon, S.A., Goudeau, D., Malmstrom, R.R., Woyke, T., and Orphan, V.J., (2016) Visualizing in situ translation activity for identifying and sorting slow-growing archaeal-bacterial consortia. *Proc Natl Acad Sci USA* **113:** E4069–E4078.

Heldal, M., and Bratbak, G. (1991) Production and decay of viruses in aquatic environments. *Mar Ecol Prog Ser* **72:** 205–212.

Helton, R.R., Cottrell, M.T., Kirchman, D.L., and Wommack, K.E. (2005) Evaluation of incubation-based methods for estimating virioplankton production in estuaries. *Aquat Microb Ecol* **41:** 209–219.

Hennes, K.P., Suttle, C.A., and Chan, A.M. (1995) Fluorescently labeled virus probes show that natural virus populations can control the structure of marine microbial communities. *Appl Environ Microbiol* **61:** 3623–3627.

Hewson, I., Govil, S.R., Capone, D.G., Carpenter, E.J., and Fuhrman, J.A. (2004) Evidence of Trichodesmium viral lysis and potential significance for biogeochemical cycling in the oligotrophic ocean. *Aquat Microb Ecol* **36:** 1–8.

Holmfeldt, K., Solonenko, N., Shah, M., Corrier, K., Riemann, L., VerBerkmoes, N.C., *et al.* (2013) Twelve previously unknown phage genera are ubiquitous in global oceans. *Proc Natl Acad Sci USA* **110:** 12798–12803.

Hurwitz, B.L., Brum, J.R., and Sullivan, M.B. (2015) Depth-stratified funcational and taxonomic niche specialization in the 'core' and 'flexible' Pacific Ocean Virome. *ISME J* **9:** 472–484.

Kang, I., Oh, H.-M., Kang, D., and Cho, J.-C. (2013) Genome of a SAR116 bacteriophage shows the prevalence of this phage type in the oceans. *Proc Natl Acad Sci USA* **110:** 12166–12167. \

Kopf, S.H., McGlynn, S.E., Green-Saxena, A., Guan, Y., Newman, D.K., Orphan, V.J., (2015) Heavy water and 15N labeling with nanoSIMS analysis reveals growth rate-dependent metabolic heterogeneity in chemostats. *Environ Microbiol* **17:** 2542–2556.

Mackinder, L.C.M., Worthy, C.A., Biggi, G., Hall, M., Ryan, K.P., Varsani, A., *et al.* (2009) A unicellular algal virus, Emiliania huxleyi virus 86, exploits an animal-like infection strategy. *J Gen Virol* **90:** 2306–2316.

Massana, R., del Campo, J., Dinter, C., and Sommaruga, R. (2007) Crash of a population of the marine heterotrophic flagellate *Cafeteria roenbergensis* by viral infection. *Environ Microbiol* **9:** 2660–2669.

Moniruzzaman, M., Wurch, L.L., Alexander, H., *et al.* (2017) Virus-host relationships of marine single-celled eukaryotes resolved from metatranscriptomics. *Nat Communications* **8:** 16054. doi:10.1038/ncomms16054.

Moore, L.R., Coe, A., Zinser, E.R., Saito, M.A., Sullivan, M.B., Lindell, D., *et al.* (2007) Culturing the marine cyanobacterium Prochlorochoccus. *Limnol Oceanogr Methods* **5:** 353–362.

Musat, N., Halm, H., Winterholler, B., Hoppe, P., Peduzzi, S., Hillion, F., *et al.* (2008) A single-cell view of the ecophysiology of anaerobic phototrophic bacteria. *Proc Natl Acad Sci USA* **105:** 17861–17866.

Noble, R.T., and Fuhrman, J.A. (1998) Use of SYBR Green 1 for rapid epifluorescence counts of marine viruses and bacteria. *Aquat Microb Ecol* **14:** 113–118.

Noble, R.T., and Fuhrman, J.A. (2000) Rapid virus production and removal as measured with fluorescently labeled viruses as tracers. *Appl Environ Microbiol* **66:** 3790–3797.

Ohno, S., Okano, H., Tanji, Y., Ohashi, A., Watanabe, K., Takai, K., and Imachi, H. (2012) A method for evaluating the host range of bacteriophages using phages fluorescently labeled with 5-ethynyl-2'deoxyuridine (EdU). *Appl Microbiol Biotechnol* **95:** 777–788.

Orphan, V.J., Turk, K.A., Green, A.M., and House, C.H. (2009) Patterns of 15N assimilation and growth of methanotrophic ANME-2 archaea and sulfate reducing bacteria within structured syntrophic consortia revealed by FISH-SIMS. *Environ Microbiol* **11:** 1777–1791.

Ouverney, C.C., and Fuhrman, J.A. (2000) Marine planktonic archaea take up amino acids. *Appl Environ Microbiol* **66:** 4829–4833.

Patel, A., Nobel, R.T., Steel, J.A., *et al.* (2007) Viruses and prokaryote enumeration from planktonic aquatic environments by epifluorescence microscopy with SYBR Green 1. *Nat Protoc* **2:** 269–276.

Polerecky, L., Adam, B., Milucka, J., Musat, N., Vagner, T., and Kuypers, M.M. (2012) Look@ NanoSIMS–a tool for the analysis of nanoSIMS data in environmental microbiology. *Environ Microbiol* **14:** 1009–1023.

Proctor, L.M., Okubo, A., and Fuhrman, J.A. (1993) Calibrating estimates of phage induced mortality in marine bacteria: ultrastructural studies of marine bacteriophage development from one-step growth experiments. *Microb Ecol* **25:** 161–182.

Rippka, R. (1988) Isolation and purification of cyanobacteria. *Methods Enzymol* **167:** 3–27.

Roux, S., Brum, J.R., and Dutilh, B.E. (2016a) Ecogenomics and potential biogeochemical impacts of globally abundant ocean viruses. *Nature* **537:** 289–693.

Roux, S., Solonenko, N., Dang, V.T., Poulos, B.T., Schwenck, S.M., Goldsmith, D.B., *et al.* (2016b) Towards quantitative viromics for both double-stranded and single-stranded DNA viruses. *PeerJ* **4:** e2777.

R Development Core Team. (2013). *R: A Language and Environment for Statistical Computing*. Vienna, Austria: R Foundation for Statistical Computing. URL http://www.R-project.org

Samo, T.J., Smriga, S., Malfatti, F., Sherwood, B.P., and Azam, F. (2014) Broad distribution and high proportion of protein synthesis active marine bacteria revealed by click chemistry at the single cell level. *Front Mar Science Aquat Microbiol* **1:** 48. doi:10.3389/fmars.2014.00048

Schroeder, D.C., Oke, J., Malin, G., and Wilson, W.H. (2002) Coccolithovirus (Phycodnaviridae): characterisation of a new large dsDNA algal virus that infects Emiliana huxleyi. *Arch Virol* **147:** 1685–1698.

Sheik, A.R., Brussaard, C.P.D., Lavik, G., Foster, R.A., Musat, N., Adam, B., *et al.* (2013) Viral infection of *Phaeocystis globosa* impedes release of chitinous star-like structures:

quantification using single cell approaches. *Environ Microbiol* **15:** 1441–1451.
Sheik, A.R., Brussaard, C.P.D., Lavik, G., Lam, P., Musat, N., Krupke, A., *et al*. (2014) Response of the coastal bacterial community to viral infection of the algae *Phaeocystis globosa*. *ISME J* **8:** 212–225.
Sherr, B.F., Sherr, E.B., and Fallon, R.D. (1987) Use of monodispersed, fluorescently labeled bacteria to estimate in situ protozoan bacterivory. *Appl Environ Microbiol* **53:** 958–965.
Steward, G.F., Wikner, J., Smith, D.C., Cochlan, W.P., and Azam, F. (1992a) Estimation of virus production in the sea: I. Method development. *Mar Microb Food Webs* **6:** 57–78.
Steward, G.F., Wikner, J., Cochlan, W.P., Smith, D.C., and Azam, F. (1992b) Estimation of virus production in the sea: II. Field Results. *Mar Microb Food Webs* **6:** 79–90.
Steward, G.F.D., Smith, C., and Azam, F. (1996) Abundance and production of bacteria and viruses in the Bering and Chukchi seas. *Mar Ecol Prog Ser* **131:** 287–300.
Steward, G.F., Culley, A.I., Mueller, J.A., Wood-Charlson, E.M., Belcaid, M., Poisson, G. (2013) Are we missing half of the viruses in the ocean?. *ISME J* **7:** 672–679.
Sullivan, M.B., Waterbury, J.B., and Chisholm, S.W. (2003) Cyanophages infecting the oceanic cyanobacterium Prochlorococcus. *Nature* **424:** 1047–1051.
Suttle, C.A. (2005) Viruses in the sea. *Nature* **437:** 356–361.
Suttle, C.A. (2007) Marine viruses– major players in the global ecosystem. *Nat Rev Microbiol* **5:** 801–812.
Terrado, R., Pasulka, A.L., Lie, A.A.Y., Orphan, V.J., Heidelberg, K.B., Caron, D. A. (2017) Autotrophic and heterotrophic acquisition of carbon and nitrogen by a mixotrophic chrysophyte established through stable isotope analysis. *ISME J* **11:** 2022–2034.
Wang, A., Winblade Nairn, N., Johnson, R.S., Tirrell, D.A., and Grabstein, K. (2008) Processing of N-terminal unnatural amino acids in recombinant human interferon-β in *Escherichia coli*. *Chem BioChem* **9:** 324–330.
Waterbury, J.B., Watson, S.W., Valois, F.W., and Franks, D.G. (1986) Biological and ecological characterization of the marine unicellular cyanobacteria *Synechococcus*. *Can Bull Fish Aquat Sci* **214:** 71–120.
Waterbury, J.B., and Willey, J.M. (1988) Isolation and growth of marine planktonic cyanobacteria. *Methods Enzymol* **167:** 100–105.
Waters, J.C. (2009) Accuracy and precision in quantitative fluorescence microscopy. *J Cel Biol* **185:** 1135–1148.
Weber, R.J.M., Selander, E., Sommer, U., and Viant, M.R. (2013) A stable-isotope mass spectrometry-based metabolic footprinting approach to analyze exudates from phytoplankton. *Mar Drugs* **11:** 4158–4175.
Weinbauer, M.G. (2004) Ecology of prokaryotic viruses. *FEMS Microbiol Rev* **28:** 127–181.
Weinbauer, M.G., Rowe, J.M., and Wilhelm, S.W. (2010) Determining rates of virus production in aquatic systems by the virus reduction approach. In *Manual of Aquatic Virus Ecology*. Wilhelm, S.W., Weinbauer, M.G., Suttle, C.A. (eds). Waco, TX: ASLO, pp. 1–8.
Weitz, J.S., and Wilhelm, S.W. (2012) Ocean viruses and their effects on microbial communities and biogeochemical cycles. *F1000 Biol Rep* **4:** 17.
Wilhelm, S.W., Brigden, S.M., and Suttle, C.A. (2002) A dilution technique for the direct measurement of viral production: a comparison in stratified and tidally mixed coastal waters. *Microb Ecol* **43:** 168–173.
Wilhelm, S.W., and Suttle, C.A. (1999) Viruses and nutrient cycles in the sea. *BioScience* **49:** 781–788.
Winget, D.M., Williamson, K.E., Helton, R.R., and Wommack, K.E. (2005) Tangential flow diafiltration: an improved technique for estimation of virioplankton production. *Aquat Microb Ecol* **41:** 221–232.
Wiśniewski, J.R., Zougman, A., Nagaraj, N., and Mann, M. (2009) Universal sample preparation method for proteome analysis. *Nat Methods* **6:** 359–363.
Woebken, D., Burow, L.C., Prufert-Bebout, L., Bebout, B.M., Hoehler, T.M., Pett-Ridge, J., *et al*. (2012) Identification of a novel cyanobacterial group as active diazotrophs in a coastal microbial mat using nanoSIMS analysis. *ISME J* **6:** 1427–1439.
Wommack, K.E., and Colwell, R.R. (2000) Virioplankton: viruses in aquatic ecosystems. *Microbiol Mol Biol Rev* **64:** 69–114.
Vardi, A., Haramaty, L., Van Mooy, B.A.S., Fredricks, H.F., Kimmance, S.A., Larsen, A., *et al*. (2012) Host-virus dynamics and subcellular controls of cell face in natural coccolithophore populations. *Proc Natl Acad Sci USA* **109:** 19327–19332.
Vizcaíno, J.A., Csordas, A., del-Toro, N., Dianes, J.A., Griss, J., Lavidas, I., *et al*. (2016) 2016 update of the PRIDE database and related tools. *Nucleic Acids Res* **44:** D447–D456. PubMed ID: 26527722).
Yildiz, A., and Selvin, P.R. (2005) Fluorescence imaging with one nanometer accuracy: application to molecular motors. *Acc Chem Res* **38:** 574–582.
Zhang, S.L., Tan, H.C., Hanson, B.J., and Ooi, E.E. (2010) A simple method for Alexa Fluor dye labeling of dengue virus. *J Viriol Methods* **167:** 172–177.
Zhao, Y., Temperton, B., Thrash, J.C., Schwalbach, M.S., Vergin, K.L., Landry, Z.C., *et al*. (2013) Abundant SAR11 viruses in the ocean. *Nature* **494:** 357–360.

Supporting information

Additional Supporting Information may be found in the online version of this article at the publisher's web-site:

Fig. S1. Estimated Instrument isotope fractionation factors for each analytical session (e.g., run date). Fractionation factors were calculated from the deviation in isotope rate of all unlabelled ROIs (viruses and hosts) relative to the expected ratio (approximately natural abundance, 13C*n*at = 0.011 and 15N*n*at = 0.0036). These fractionation factors were used to correct all measured collected during each analytical session.

Fig. S2. Compiled nanoSIMS isotope data from adsorption controls. Whisker Plots showing adsorption controls of coccolithophore *E. huxleyi* using 15N-ammonium (leP panel) and 15N-nitrate (middle panel) relative to unlabelled controls (right panel). Fractional abundance (*y*-axis) Reveals enrichment above natural abundance (indicated with thicker grey line at 0.36 at %).

Fig. S3. Scarer Plots revealing total ion counts for hosts and viruses. Ion counts of 12C And 14N12C For individual

host and viral particles in one analytical frame (A, C) And averaged across all analytical frames for each measurement spot (B, D). These Plots demonstrate the increased error with low ion counts and the value of averaging across planes to reduce this error.

Fig. S4. Growth of host cells in HPG. Concentration of *E. coli* (as Determined by optical density; OD 600) (A) and *E. Huxleyi* (B) Over time aPer HPG addition (red arrow) and viral particles (blue arrow). In the case of *E. huxleyi*, two cultures were grown up for 24 h with either HPG (or DMSO In the case of the – HPG treatments) prior to the data shown. These cultures were then split to create the four treatments with and without viruses. Additional HPG (or DMSO) was added at this time.

Fig. S5. Demonstration of image analysis for viral particles of different size ranges. Epifluorescent Images T7 (A), Syn1 (B) and EhV 207 (C) particles stained with SYBR Gold And histogram of particle size distribution for each virus (D). Average particle size (as Determine by green fluorescence and indicated with dashed line) was 0.24, 0.4 and 0.4 μM for T7, Syn1 and EhV respectively. Images and histogram demonstrate the ability to visualize viral particles ranging from 50 to 200 Nm using SYBR Gold, but confirm that fluorescence size data is not an accurate measure of capsid diameter. Insets demonstrate viral particle selection using Matlab image analysis. The ability to resolve two individual particles from one another is set by the objective (UPLFLN 100X 1.3 NA; 0.26 μM resolution). The pixel resolution is set by the CCD camera (QIClick 12-bit Model 01-QICLICK-R-F-M-12; 1 Pixel $\approx$ 0.1159 μM). By Selng a conservative upper size limit for quantitative analysis (e.g., 0.45 μM), all viral particles in the correct size range are considered, but actual size data can not be interpreted as real for any aspect of the analysis.

Fig. S6. Results of Viral BONCAT sensitivity testing. Exploring the influence of *n*subs, *d*RG and the % Of the viral population actively turning over on the *R:G* distributions. Blue shaded area represents ideal range of parameters to detect viral production. Red Shaded area indicates range of parameters for which Viral BONCAT Can not accurately determine viral production (e.g., HPG incorporation is not distinguishable from negative control).

Fig. S7. Results of Viral BONCAT sensitivity testing. Results of Viral BONCAT sensitivity testing. Exploring The influence of *n*subs, *d*RG and different levels of variability around the *d*RG on the *R:G* distribution of the when 99% Of the viral population is actively turning over. The T7 positive HPG distribution is most accurately matched when *n*subs = 12, dRG = 0.05 and there is 60% Variability around the *d*RG.

Fig. S8. Accuracy and precision of viral production estimates using Viral BONCAT. Results from modelling T7 Data with a specific level of activity (e.g., the percent of the population actively turning over) and varying *n*sub, *d*RG and different levels of variability around the *d*RG to determined the ability to back calculate the original activity using the rank-sum bootstrap approach. This figure includes systematic noise in *R:G* up to 0.01 (10%), enlarging the confidence intervals around each estimate.

Table S1. Methionine content for viral model systems. Data derived from the following sources:T7—hRp://www.uniprot.org/uniprot/?query-organism:10760+keyword:1185;EhV207—hRps://www.ncbi.nlm.nih.gov/nuccore/JF974317.1;Syn1—hRps://www.ncbi.nlm.nih.gov/nuccore/GU071105